SWC-TR-61-90

HEADQUARTERS
AIR FORCE SPECIAL WEAPONS CENTER
AIR FORCE SYSTEMS COMMAND
KIRTLAND AIR FORCE BASE, NEW MEXICO

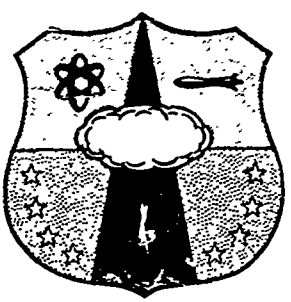

STUDIES OF RESPONSE OF ARCHES AND DOMES UNDER DYNAMIC LOADS

by

T. Huang
S. Iyengar
R. L. Jennings

October 1961

University of Illinois
Department of Civil Engineering

HEADQUARTERS
AIR FORCE SPECIAL WEAPONS CENTER
Air Force Systems Command
Kirtland Air Force Base
New Mexico

TR-61-90

STUDIES OF RESPONSE OF ARCHES AND DOMES UNDER DYNAMIC LOADS

by

T. Huang
S. Iyengar
R. L. Jennings

October 1961

Approved by
A. R. Robinson and A. S. Veletsos

University of Illinois
Department of Civil Engineering

Research Directorate
AIR FORCE SPECIAL WEAPONS CENTER
Air Force Systems Command
Kirtland Air Force Base
New Mexico

Approved.

DONALD I. PRICKETT
Colonel USAF
Director, Research Directorate

Project 1080
Task 108002
Contract AF 29(601)-2591

ABSTRACT

This report, consisting of Parts I, II and III, is concerned with three different aspects of the response of arches and domes under dynamic loads.

In Part I the accuracy of an approximate design method for arches subjected to dynamic loads is evaluated by comparing the predictions of this method with the exact solutions. Primary emphasis is placed on the effects of loads which are uniformly distributed around the arch.

In Part II the response of circular elastic arches under a moving pressure pulse is investigated by the modal method of analysis. Various combinations of natural modes are considered, and the combination of the smallest number of modes which satisfactorily approximates the exact solution is determined. It is concluded that good approximation to the true response can be obtained by considering the contributions of the first antisymmetrical and the first two symmetrical natural modes of vibration.

Part III presents a derivation of an approximate theory for the dynamic response of spherical shells loaded unsymmetrically by time-varying pressures. Non-linear effects are considered so that the resulting equations reflect the buckling tendencies associated with large-deflection behavior.

PUBLICATION REVIEW

This report has been reviewed and is approved.

FOR AND IN THE ABSENCE OF
JOHN J. DISHUCK
Colonel USAF
Deputy Chief of Staff for Operations

PART I

EVALUATION OF A DESIGN METHOD FOR ARCHES SUBJECTED TO DYNAMIC LOADS

by

Tseng Huang

Approved by

A. S. Veletsos

EVALUATION OF A DESIGN METHOD FOR ARCHES SUBJECTED TO DYNAMIC LOADS

1. Object and Scope

The purpose of the study described in this part of the report was to evaluate the accuracy of the design method presented in Reference 1* for arches subjected to the pressures associated with an atomic explosion. The approach used consists of evaluating the response of several arches by this method and comparing the results with those obtained on the basis of the method reported in Reference 2. In the latter method, the actual arch is replaced by a discrete framework consisting of a series of rigid bars, flexible joints, and concentrated point masses. For the sake of brevity, this method will be referred to as the "exact" method, and the method of Ref. 1 as the approximate method.

The solutions presented are for two-hinged, circular, elastic arches of uniform cross section. The majority of the solutions are for a uniform all-around pressure with a time-wise variation represented by a triangle with an initial peak. Some results are also presented for a triangular pressure pulse moving across the arch.

Inasmuch as Reference 1 is not readily available, a brief description of the approximate method is given in the following section. The "exact" method is described in detail in Reference 2.

2. Review of Approximate Method

In this method the actual loading on the arch is separated into a symmetrical component and an antisymmetrical component, as shown in Fig. 1. The intensity of the pressure for the symmetrical component, p_c, is considered to be constant around the arch. Similarly, for the antisymmetrical component, the pressure intensities, p_a, for the windward and leeward sides are considered to be equal but of opposite sign.

---

* Reference figure and equation numbers refer to those in each part of the report.

The response under the symmetrical component of loading is evaluated by considering two modes of deformation:

(a) The "uniform compression" mode, which is considered to produce a uniform compression without any bending, and

(b) The "bending-compression" mode in which the arch bends inward at the crown and outward near the haunches. It is assumed that the bending moment at the crown is due to this mode only.

The intensity of the load associated with the uniform compression mode is taken as the intensity of the symmetrical load component, whereas the intensity of the load associated with the compression-bending mode is taken as one-third of that for the uniform compression mode.

The response due to the antisymmetrical component of loading is evaluated by considering the so-called "deflection mode" which is antisymmetrical about the crown. Thus the computation of the response in each mode involves the analysis of a single-degree-of-freedom system.

The natural periods of the arch in the various modes of deformation are determined as follows: For a circular arch with uniform cross section, the natural period of the uniform compression mode, T_{uc}, is taken as

$$T_{uc} = 2\pi\sqrt{\frac{mR^2}{EA}} \qquad (1)$$

where m denotes the mass per unit of length of the arch, R the radius of the arch, A the cross sectional area, and E the modulus of elasticity of the material of which the arch is composed.

The period of the bending-compression mode for no thrust in the arch, T'_{cb}, is taken equal to the period of a simply supported beam having a span equal to one-third the arc length of the arch, i.e.

$$T'_{cb} = \frac{2L_{cb}^2}{\pi}\sqrt{\frac{m}{EI}} \tag{2}$$

where

$$L_{cb} = \frac{R\,\varphi_o}{3} \tag{3}$$

The symbol φ_o denotes the angle of opening of the arch, as shown in Fig. 1. The prime on T_{cb} is used to indicate that the effect of the thrust is not considered in this expression.

The corresponding period of the deflection mode, T'_d, is taken as

$$T'_d = C_1 \frac{2L_d^2}{\pi}\sqrt{\frac{m}{EI}} \tag{4}$$

where

$$L_d = \frac{R\,\varphi_o}{2} \tag{5}$$

and C_1 is a correction factor accounting for the fact that the arch does not act entirely as a beam. The following expressions are given for C_1: For a hinged arch,

$$C_1 = \frac{n^2 + 1.5}{n^2 - 1}, \tag{6a}$$

and for a fixed arch

$$C_1 = \frac{n^2 + 1}{n^2 - 0.5} \tag{6b}$$

where

$$n = \frac{2\pi}{\varphi_o} \tag{7}$$

The "actual" periods, T_{cb} and T_d, which incorporate the effect of the thrust, are determined approximately by multiplying the values of T'_{cb} and T'_d by the factor

$$\frac{1}{1 - \frac{\bar{p}}{p_{cr}}}$$

where $\bar{p}$ is the intensity of the "model pressure" on the arch at the instant that the corresponding model displacement is maximum and p_{cr} is the critical static buckling pressure. For a hinged arch, p_{cr} is given by the equation

$$p_{cr} = \left[\frac{4\pi^2}{\varphi_o^2} - 1\right] \frac{EI}{R^3} \tag{8}$$

With the intensity of the loading and the value of the natural period of vibration for each mode of deformation determined, the response of the arch in each of these modes is evaluated by analyzing the arch as a system with a single degree of freedom.

For an arch subjected to the symmetrical component of loading shown in Fig. 1, the axial force associated with the uniform compression mode is determined from the equation

$$N = (A.F.)_N \, p_c R \, , \tag{9}$$

where $p_c R$ is approximately the force produced under static conditions, and $(A.F.)_N$ is the amplification factor for N. This factor depends on the shape of the applied pressure and the ratio of the duration of the pulse to the natural period of vibration of the particular mode of deformation considered. The maximum bending moment associated with the bending-compression mode occurs at the quarter points of the arch, and may be expressed as

$$M = (A.F.)_M \, M_s \tag{10}$$

where the static moment, M_s, is taken as

$$M_s = \frac{\varphi_o^2(R/r)}{216} p_c Rr \cdot \frac{1}{1 - (\frac{\varphi_o}{3\pi})^2} \qquad (11)$$

The first factor on the right side of this expression represents the maximum moment in a simply supported beam having a span length L_{cb}, as defined by Eq. (3), and subjected to a uniform static pressure of intensity $p_c/3$. The symbol r represents the radius of gyration of the cross section of the arch. The second factor accounts for the effect of arch curvature. The amplification factor $(A.F.)_M$ must be determined on the basis of the period of the compression-bending mode, T'_{cb}.

For the antisymmetrical component of loading shown in Fig. 1, the bending moment is determined from Eq. (10). However, the amplification factor must be based on the period of the deflection mode T'_d, and the static moment must be determined for a pressure p_d and a length L_d as given by Eq. (5). For a hinged arch, the expression for M_s becomes

$$M_s = \frac{\varphi_o^2(R/r)}{32} p_d Rr \cdot \frac{1}{1 - (\frac{\varphi_o}{2\pi})^2} \qquad (12)$$

The effect of the axial thrust is taken into account in figuring the bending resistance of the arch. For the compression bending mode, the bending resistance is taken as the product of the corresponding resistance for no thrust multiplied by the factor

$$1 - \bar{p}/p''_{cr}$$

where p''_{cr} is the buckling load corresponding to a length $L_{bc} = R\varphi_o/3$. For the deflection mode, the reduction factor is taken as

$$1 - \bar{p}/p_{cr}$$

where p_{cr} is as previously defined. The inverse of these factors can also be interpreted as magnification factors to be applied to Eq. (10).

3. Results of Comparisons for Arches Under Uniform Pressure

3.1 General. The response curves presented in the remainder of this part of the report are for two-hinged circular elastic arches of uniform cross section subjected to a uniform all-around pressure pulse. The pressure-time relationship is represented by an initially peaked triangle, as shown in the upper left corner of Fig. 2a. The peak intensity of the pressure is denoted by p_o and the duration of the pulse by t_d. The values of these quantities are specified in terms of the dimensionless ratios p_o/p_{cr} and t_d/T_o, where P_{cr} represents the critical buckling pressure corresponding to an antisymmetrical mode of deformation, and T_o represents the breathing period of vibration of a complete ring having the same radius and cross section as the arch.

It has been shown (Ref. 2) that, for the conditions considered, the axial force in the arch is fairly uniform along the arch and that the maximum moment occurs at the crown. In view of this, only the moment and the axial force at the crown will be considered.

Since the arch is uniformly loaded, in the application of the approximate method, only the uniform compression mode and the bending-compression mode need be considered. The former mode yields the axial force in the arch, and the latter gives the moment at the crown. For the triangular pulse investigated, the amplification factor, A.F., for an elastic system that is initially at rest is given by the following equations:

For $t \leq t_d$,

$$A.F. = 1 - \frac{t}{t_d} - \cos 2\pi \frac{t}{T} + \frac{1}{2\pi} \frac{T}{t_d} \sin 2\pi \frac{t}{T} \qquad (13)$$

For $t \geq t_d$,

$$A.F. = \sqrt{A^2 + B^2} \sin \left(2\pi \frac{t - t_d}{T} + \alpha\right) \tag{14a}$$

where

$$A = \cos 2\pi \frac{t_d}{T} + \frac{1}{2\pi} \frac{T}{t_d} \sin 2\pi \frac{t_d}{T} \tag{14b}$$

$$B = -\frac{1}{2\pi} \frac{T}{t_d} \left(1 - \cos 2\pi \frac{t_d}{T}\right) + \sin 2\pi \frac{t_d}{T} \tag{14c}$$

$$\alpha = \tan^{-1} \frac{A}{B} \tag{14d}$$

In the above expressions, the quantity T denotes the natural period of the particular mode of deformation considered.

3.2 Comparison of Typical Response Curves. In Fig. 2 are shown the time-histories of the axial force and the bending moment at the crown of a two-hinged arch with the following dimensions:

Rise-to-Span Ratio = f/L_o = 0.20 (corresponds to $\varphi_o = 87.21^\circ$)

Slenderness Ratio = L_o/r = 100 (corresponds to $R/r = 72.5$)

The intensity of the peak pressure and the duration of the pulse are as follows:

$$p_o/p_{cr} = 1 \quad \text{and} \quad t_d/T_o = 2$$

The dashed curve, reproduced from Reference 2, may be considered to represent the exact solution. The solid curve was obtained by the approximate method.

From Fig. 2a it can be seen that, except for a slight phase difference which is of no importance from a design point of view, the approximate solution for the axial force is in very good agreement with the "exact" solution. Included in this figure is also the solution obtained by replacing the

value of the natural period of the uniform compression mode by the value of the "extensional mode" of vibration of the arch. For the particular arch investigated, the extensional mode corresponds to the second symmetrical mode of vibration (see Fig. 4.2b of Reference 2). The use of this period does not alter the solution significantly.

In Fig. 2b, although the peak values of the bending moment determined by the two methods are in reasonable agreement, the periods of the oscillations are significantly different. The indications are that the approximate method does not account properly for the behavior of the system in bending.

In order to gain better insight into the true behavior of the system, the moment at the crown was evaluated by application of the modal method of analysis. In this analysis, the effect of the axial thrust on bending was neglected. In Fig. 3 are given the modal contributions for the first three symmetrical modes. In addition, the sum of these contributions is compared with the exact solution. It can be seen that the solution based on the first three modes is in good agreement with the exact solution. The indications are that all three contributions, particularly the one associated with the second or extensional mode, are quite important.

3.3 Effect of Pressure Intensity Parameter. In Figs. 4 and 5 are shown time histories of the axial force and the bending moment at the crown of the arch considered before, except that the intensity of the peak pressure has the values of $p_o/p_{cr} = 0.5$ and $p_o/p_{cr} = 2.0$. The other parameters of the problem are the same as those indicated in Fig. 2. The "exact" solutions presented in these and all subsequent figures are reproduced from Reference 2. In Figs. 4a and 5a, the solid curves are identical with the corresponding curve in Fig. 2a, since in the approximate method the axial

force is considered to be indeperdent of the ratio p_o/p_{cr}. It is of interest to note that the best agreement between the approximate and exact solutions for axial force is obtained for Fig. 4a which corresponds to the smallest value of p_o/p_{cr} considered. In general, the observations that can be made about the curves in Figs. 4 and 5 are similar to those made about Fig. 2.

3.4 Effect of Pulse Duration Parameter. The arch considered in the preceding section was also analyzed for values of t_d/T_o in the range between 0.25 and 4.0. In Fig. 6 are given the time-histories of the axial force and bending moment at the crown for a value of $t_d/T_o = 0.75$, and in Fig. 7 are given spectrum curves for the complete range of t_d/T_o values considered. These curves express the absolute maximum value of the axial force and bending moment at the crown as a function of the parameter t_d/T_o. Both the exact and the approximate solutions are indicated. It can be seen that the maximum axial force predicted by the approximate method is in very good agreement with that obtained by the "exact" method. On the other hand, there are significant differences between the values of the maximum moments predicted by the two methods.

3.5 Effect of Arch Dimensions. Comparative solutions were obtained for a number of arches with different dimensions. Two groups of problems were considered:

(a) Arches with a rise-span ratio, f/L_o, of 0.2, and slenderness ratios, L_o/r, of 50, 100 and 200.

(b) Arches with a value of $L_o/r = 100$ and rise-span ratios of 0.1, 0.2 and 0.5. The latter ratios correspond to values of Φ_o equal to 45.24^o, 97.21^o and 180^o, respectively. The load parameters are taken as $p_o/p_{cr} = 1$ and $t_d/T_o = 2$.

The results are summaried in Figs. 8 through 13. It can be seen that, in all cases, the peak value of the axial force predicted by the approximate method is in excellent agreement with the exact value. On the other hand, both the time histories and the peak values of the bending moments corresponding to the two methods of solution differ significantly from one another. The peak values of the bending moments are compared in Figs. 10 and 13.

4. Comparisons for Arches Subjected to a Moving Pressure Pulse

In Fig. 14 are shown the results obtained for an arch subjected to a moving pressure pulse. The pressure-time relationship was represented by an initially peaked triangle. The problem parameters were:

$$f/L_o = 0.2 \qquad L_o/r = 100$$

$$p_o/p_{cr} = 1, \qquad t_t/T_o = 1, \qquad t_d/t_t = 1$$

The quantity t_t represents the transit time, i.e. the time required for the front of the pulse to move across the arch. The remaining symbols have the same meaning as before.

In the approximate solution, the peak intensity of the symmetrical component of loading (See Fig. 1) was taken as

$$p_c = \frac{1}{1.5 + 0.5\frac{\varphi_o}{\pi}} p_o , \tag{15}$$

and the corresponding intensity of the antisymmetrical or deflection-mode component was taken as

$$p_d = \frac{0.5 + 0.5\frac{\varphi_o}{\pi}}{1.5 + 0.5\frac{\varphi_o}{\pi}} p_o \tag{16}$$

The pressure-time relationship and the duration of these component loadings were considered to be the same as those of the actual pulse.

From the results presented in Fig. 15 it can be seen that the approximate solution for the axial force is not in as good agreement with the exact solution as for the cases considered previously. It may be worth nothing, however, that in this case the stress corresponding to the maximum axial force is relatively small in comparison to that resulting from the maximum bending moment. The maximum bending moment occurs at the 3/4 point, and its peak value is predicted with reasonable accuracy, as can be seen from Fig. 14c.

In Fig. 15 are given response curves for moment at the 1/4 and 3/4 points of the arch considered before, except that the duration of the pulse is represented by a value of $t_d/t_t = 2$. It can be seen that the agreement between the solutions obtained by the two methods is fairly good, particularly when the curves corresponding to the absolute maximum effect are considered.

5. Summary

The results of the comparative studies presented can be summarized as follows:

(1) For arches subjected to a uniform radial pressure, the approximate method can predict with excellent accuracy the magnitude of the maximum axial force in the arch. However, both the time history and the magnitude of the maximum moment determined by this method may be significantly different from the exact results. The results of a modal analysis that has been made suggest that the computation of the bending moment at the crown requires consideration of the first three symmetrical modes of vibration.

(2) On the basis of the two solutions obtained for arches subjected to a triangular moving pressure, it appears that the value of the maximum moment predicted by the approximate method is in reasonable agreement with the exact value. The axial forces are not predicted as accurately

in this case as for a symmetrical load; however, this may not be very significant since the stress resulting from the maximum axial force is usually small in comparison to that due to the maximum moment.

(3) It is believed that, for elastic arches, a more rational approximate method of analysis can be developed by considering the contributions of the first two or three symmetrical modes of vibration and of the first antisymmetrical mode.

6. References

1. Newmark, N.M., "Vulnerability of Arches - Preliminary Notes," prepared for the Physical Vulnerability Division of the Directorate of Intelligence, U.S. Air Force; Department of Civil Engineering, University of Illinois, 21 May 1956 (Unpublished manuscript).

2. Eppink, R.T. and Veletsos, A.S., "Response of Arches under Dynamic Loads," University of Illinois Project, AFSWC-TR-60-53, Air Force Special Weapons Center, Kirtland Air Force Base, New Mexico, December 1960.

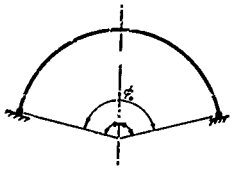

Circular Arch

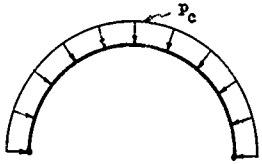

Symmetrical Component

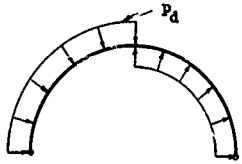

Antisymmetrical Component

FIG. 1 ARCH AND COMPONENTS OF LOADING

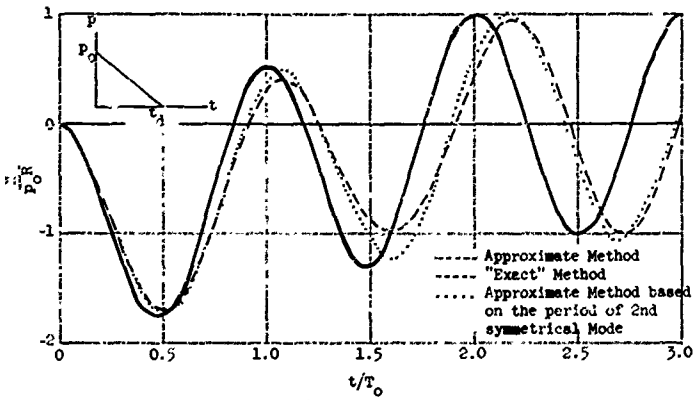

(a) Axial Force, N

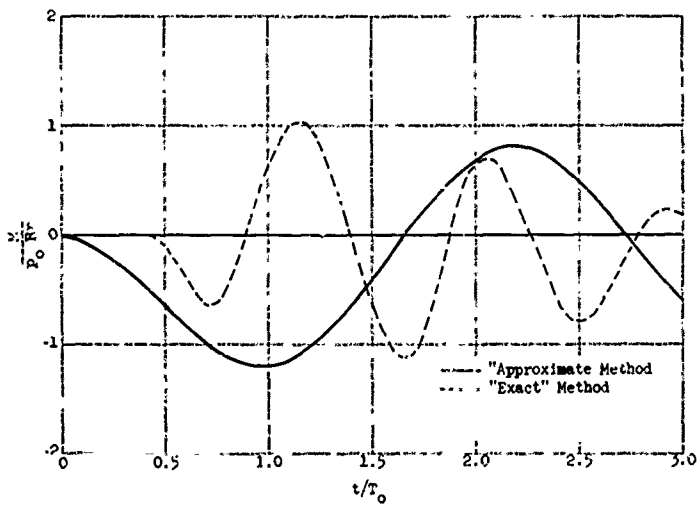

(b) Moment at Crown, .

FIG. 2 COMPARISON OF RESPONSE CURVES FOR UNIFORM PRESSURE
$f/L_o = 0.2$, $L_o/r = 100$, $p_c/p_{cr} = 1.0$, $t_1/T_o = 2.0$

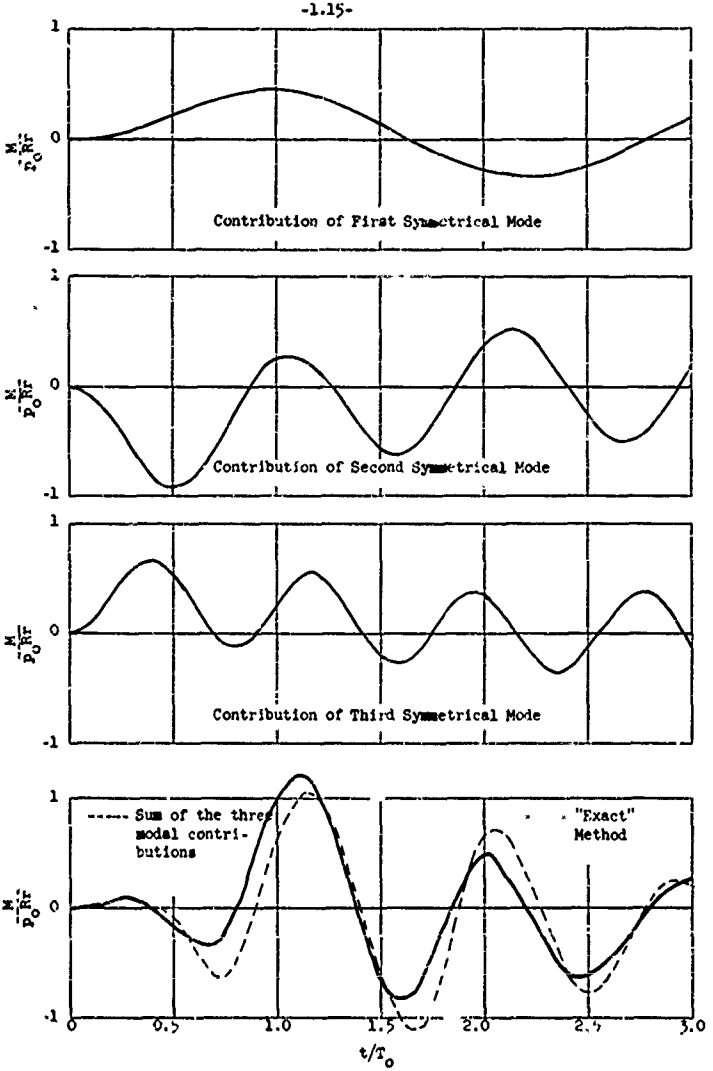

FIG. 3 MODAL CONTRIBUTIONS FOR MOMENT AT THE CROWN
Data same as in Fig. 2

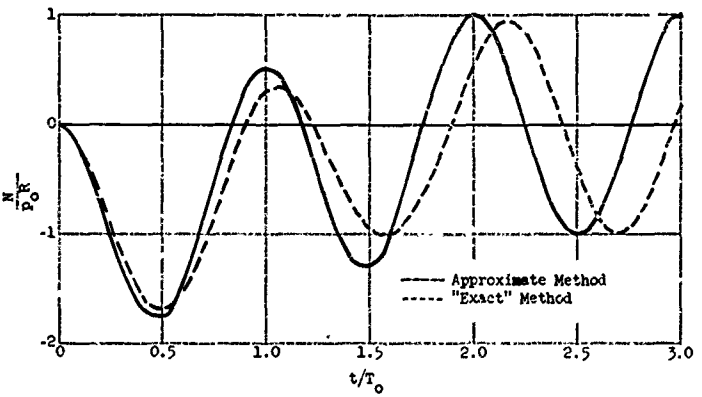

(a) Axial Force, N

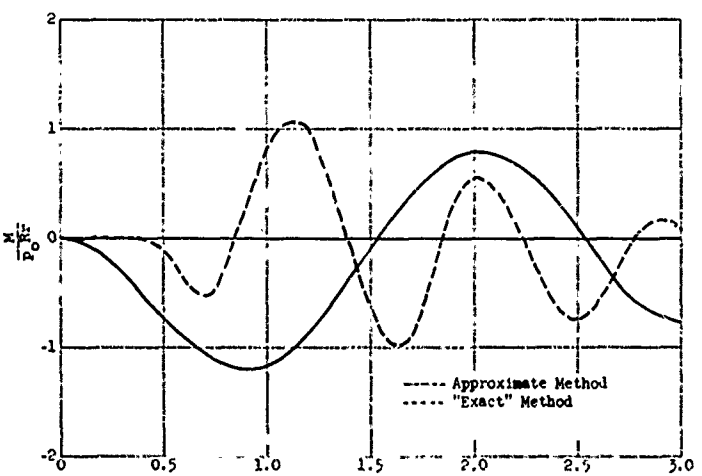

(b) Moment at Crown M

FIG. 4 COMPARISON OF RESPONSE CURVES FOR UNIFORM PRESSURE, $p_o/p_{cr} = 0.5$
Other data same as in Fig. 2

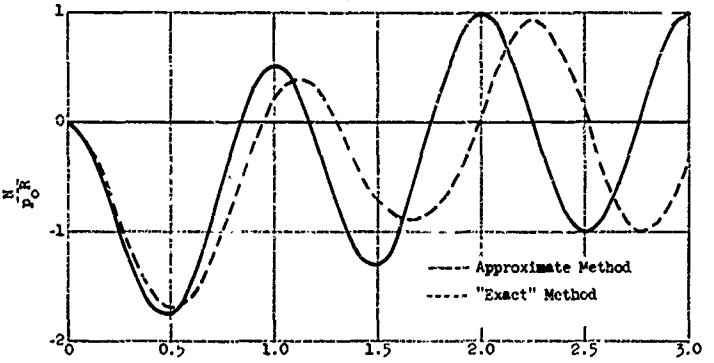

(a) Axial Force, N

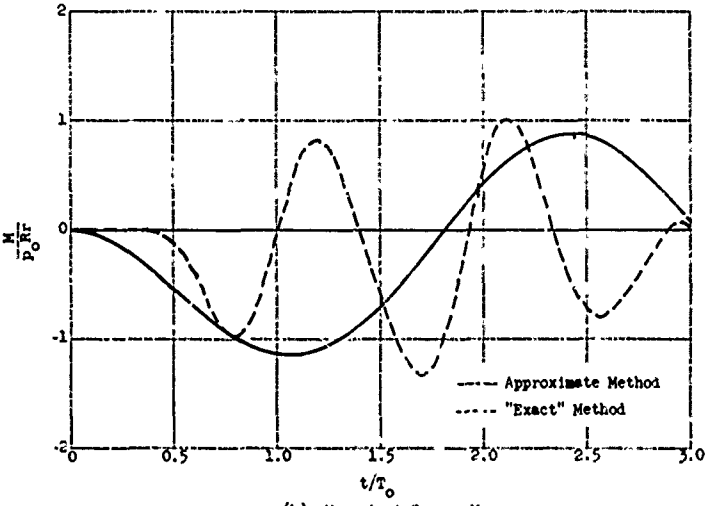

(b) Moment at Crown M

FIG. 5 COMPARISON OF RESPONSE CURVES FOR UNIFORM PRESSURE, $p_o/3_{cr} = 2.0$
Other data same as in Fig.2

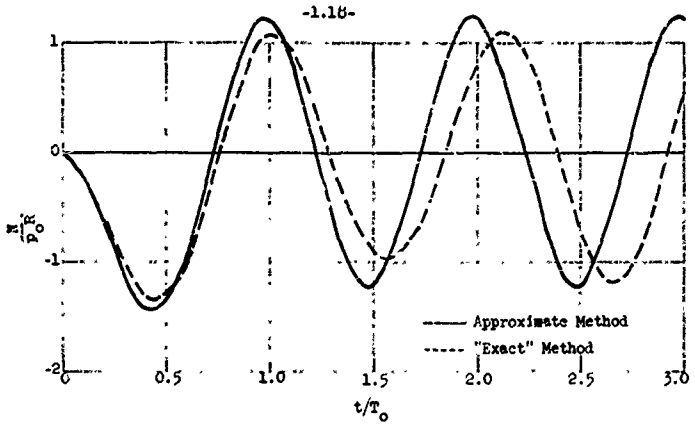

(a) Axial Force, N

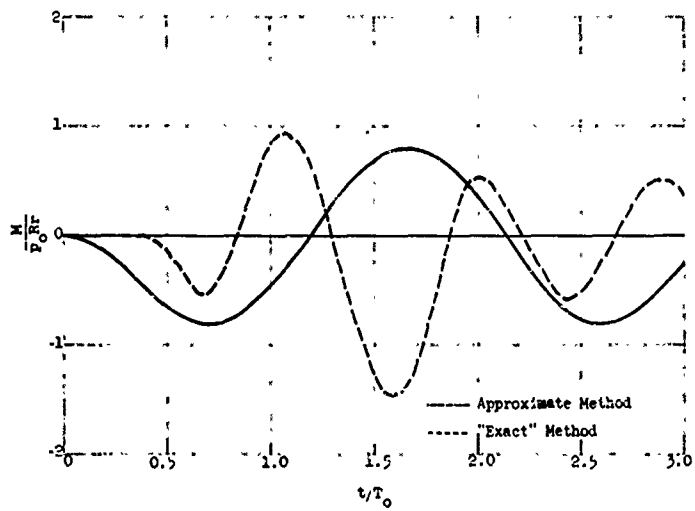

(b) Moment at Crown, M

FIG. 6 COMPARISON OF RESPONSE CURVES FOR UNIFORM PRESSURE, $t_d/T_o = 0.75$
Other data same as in Fig. 2

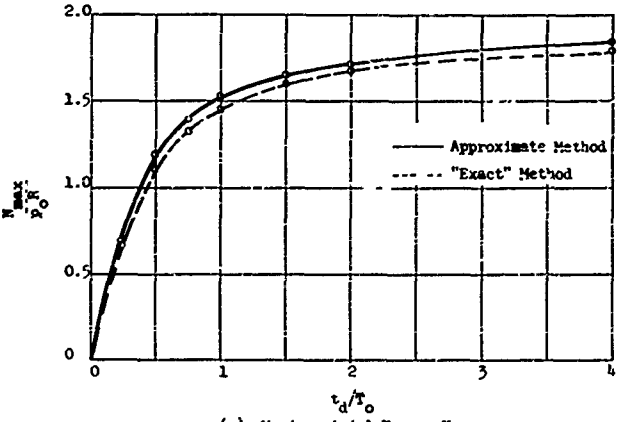

(a) Maximum Axial Force, N_{max}

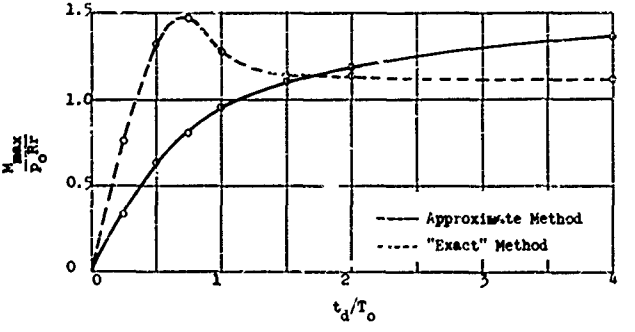

(b) Maximum Crown Moment, M_{max}

FIG. 7 COMPARISON OF RESPONSE SPECTRA--PULSE DURATION
$f/L_o = 0.2$, $L_o/r = 100$, $p_o/i_{cr} = 1.0$

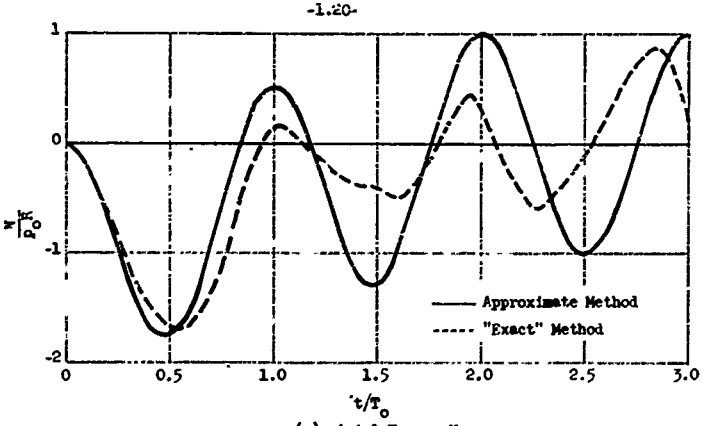

(a) Axial Force, N

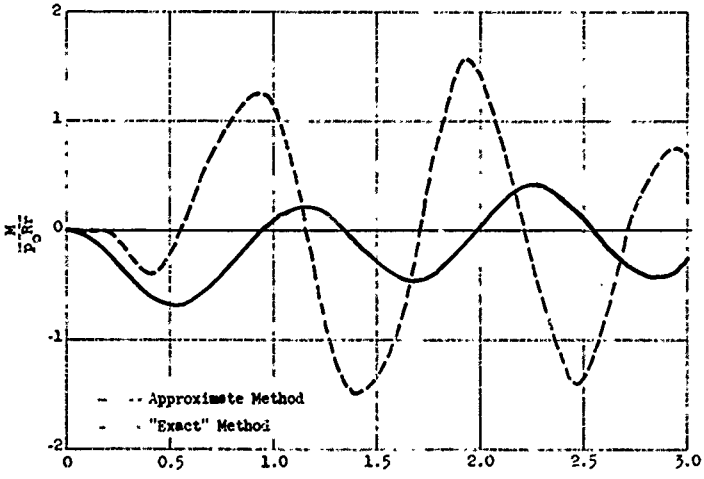

(b) Moment at Crown, M

FIG. 8 COMPARISON OF RESPONSE CURVES FOR UNIFORM PRESSURE, $L_o/r = 50$
Other data same as in Fig. 2

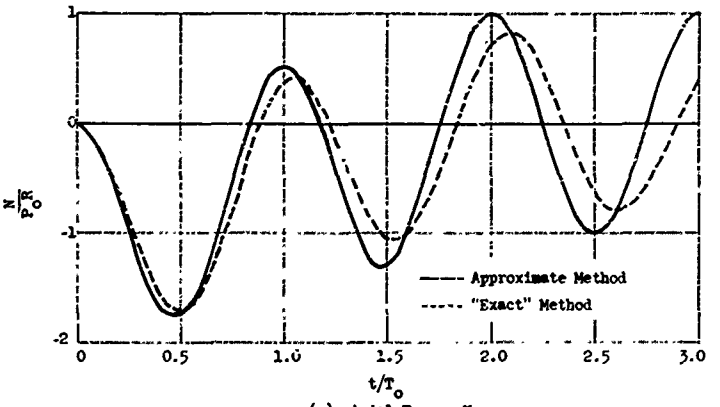

(a) Axial Force, N

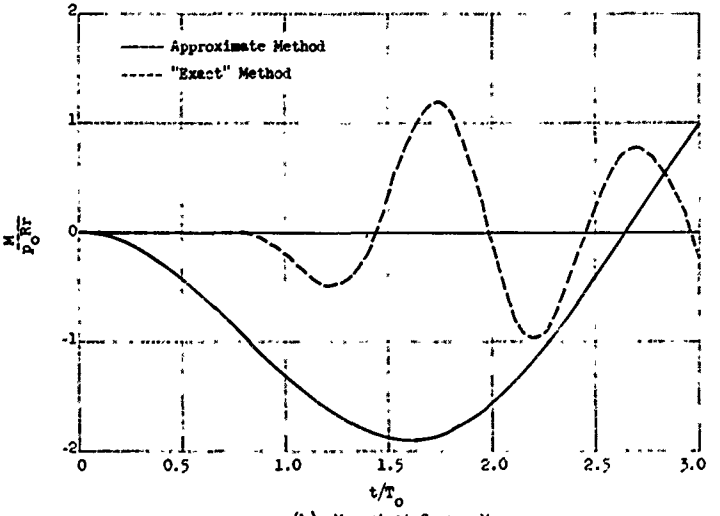

(b) Moment at Crown, M

FIG. 9 COMPARISON OF RESPONSE CURVES FOR UNIFORM PRESSURE, $L_o/r_o = 200$
Other data same as in Fig. 2

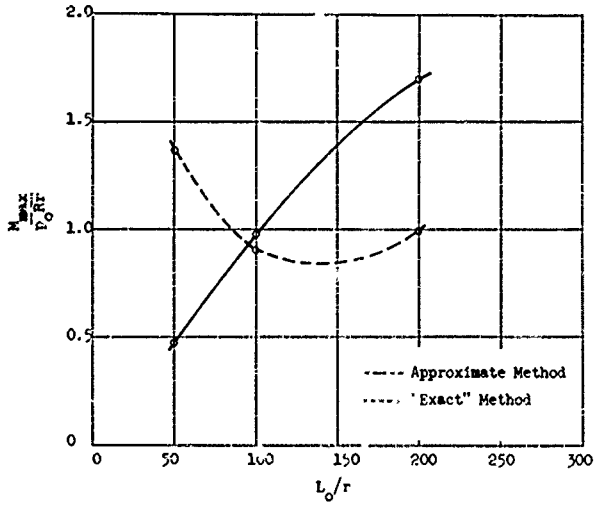

FIG. 10 COMPARISON OF SPECTRUM FOR MAXIMUM CROWN MOMENT--L_o/r VARIED
$f/L_o = 0.2$, $p_o/p_{cr} = 1.0$, $t_d/t_o = 2.0$

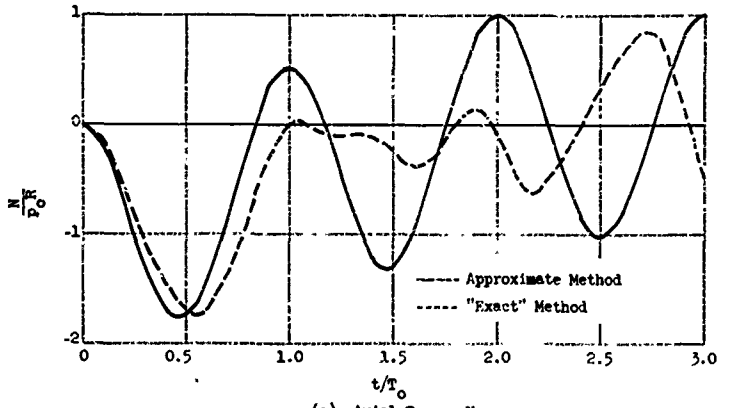

(a). Axial Force, N

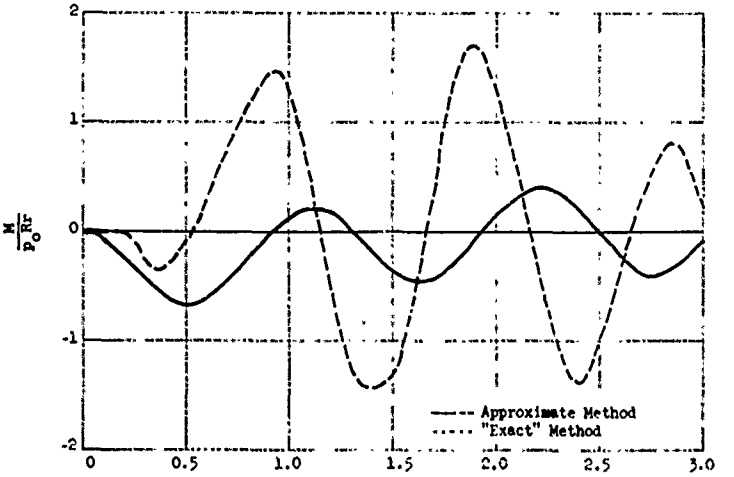

(b) Moment at Crown, M

FIG. 11 COMPARISON OF RESPONSE CURVES FOR UNIFORM PRESSURE, $t/T_o = 0.1$
Other data same as in Fig. 2

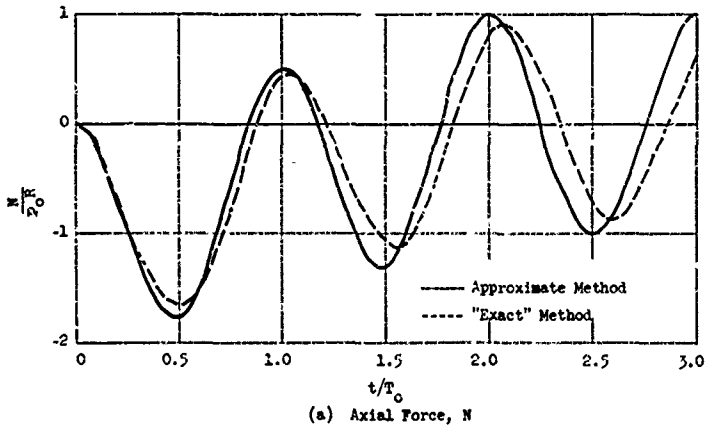

(a) Axial Force, N

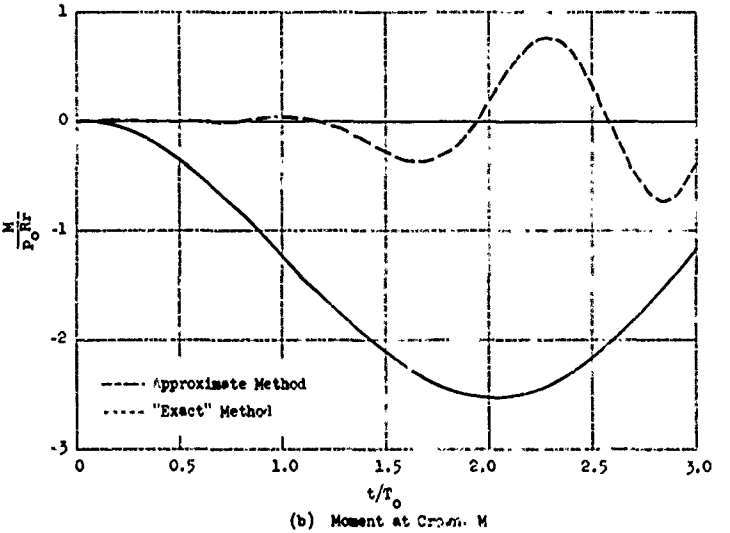

(b) Moment at Crown, M

FIG. 12 COMPARISON OF RESPONSE CURVES FOR UNIFORM PRESSURE, $f/L_o = 0.5$
Other data same as in Fig. 2

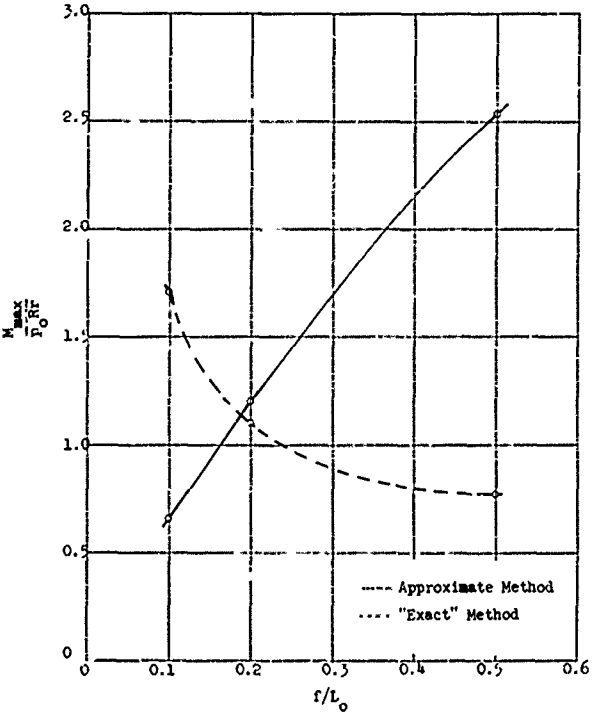

FIG. 13 COMPARISON OF SPECTRUM FOR MAXIMUM CROWN MOMENT--f/L_o VARIED

$L_o/r = 100$, $p_o/p_{cr} = 1.0$, $t_d/T_o = 2.0$

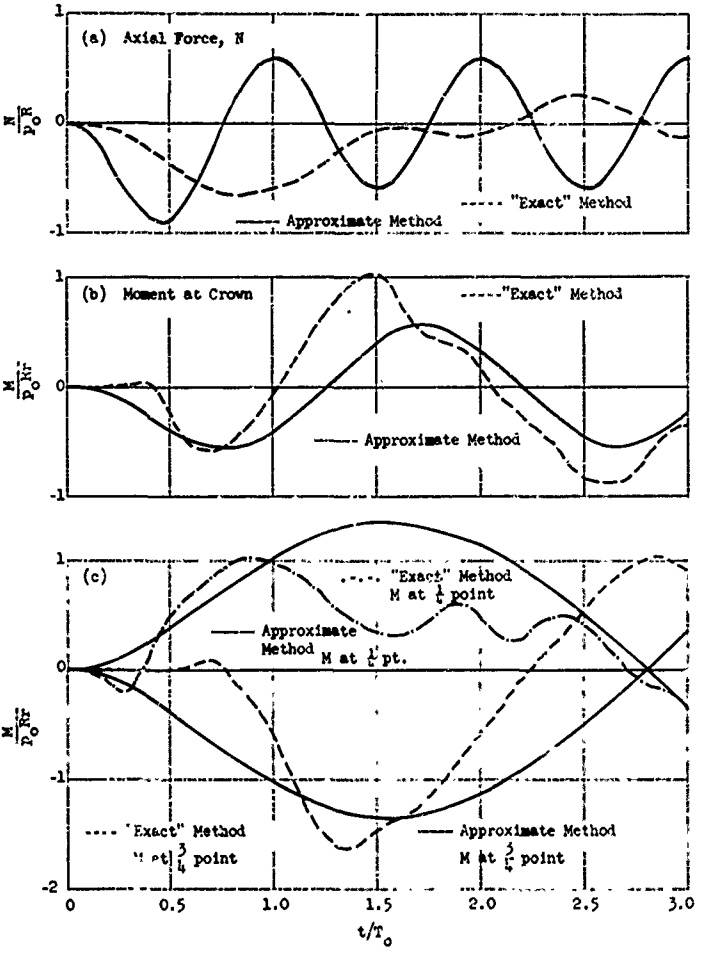

FIG. 14 COMPARISON OF RESPONSE CURVES FOR A MOVING PRESSURE PULSE
$f/L_o = 0.2$, $L_o/r = 100$, $p_o/p_{cr} = 1$, $t_t/T_o = 1$, $t_d/t_t = 1$

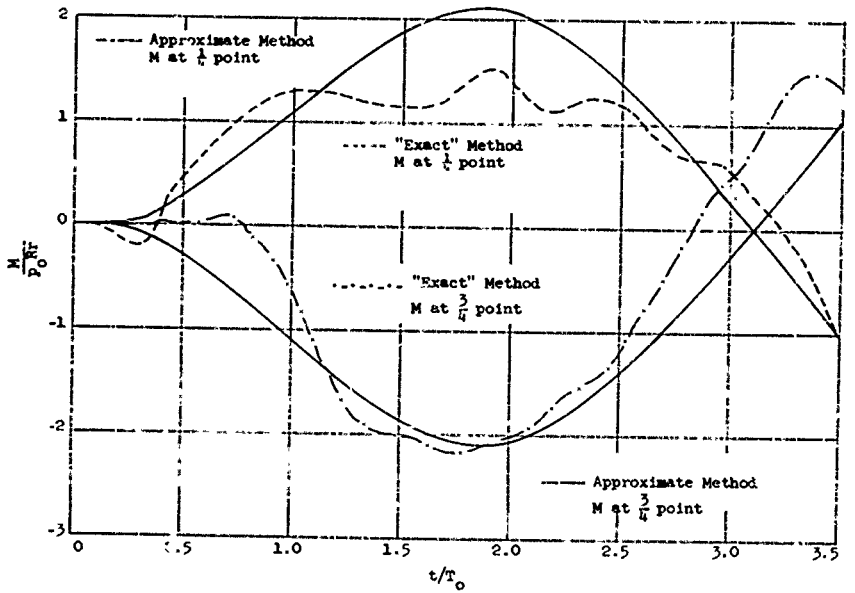

FIG. 15 COMPARISON OF MOMENT CURVES FOR A MOVING PRESSURE PULSE
$z/L_o = 0.2$, $L_o/r = 100$, $p_o/p_{cr} = 1$, $t_t/T_o = 1$, $t_d/t_t = 2$

PART II

DYNAMIC ANALYSIS OF CIRCULAR ELASTIC ARCHES BY MODAL METHOD

by

S. Iyengar

Approved by

A. S. Veletsos

DYNAMIC ANALYSIS OF CIRCULAR ELASTIC ARCHES BY MODAL METHOD

1. Object and Scope

The general purpose of this study was to investigate the dynamic response of elastic arches by application of the modal method of analysis. Specifically, it was desired to evaluate the relative contribution of the various natural modes to the total response, and to establish a basis for the development of a simplified method of analysis.

Numerical solutions have been obtained for a range of the parameters involved, and the complete solutions incorporating the contributions of all the natural modes of vibration were compared with corresponding approximate solutions obtained by considering a limited number of modes. An attempt was made to determine the combination of the smallest number of modes which best approximates the complete solution. All solutions are for two-hinged, circular, elastic arches subjected to a moving triangular pressure pulse. In the analysis, the buckling tendencies of the arch are neglected; accordingly, the response is proportional to the intensity of the applied pressure.

A digital computer program was developed for the numerical computation of the response. This program has been developed specifically for an arch subjected to a moving pressure pulse of triangular shape. The replacement system is considered to have ten bars of equal horizontal projections. A variable mode-counter set in the program makes it possible to consider any desired number of modes.

In addition to the numerical results, brief descriptions of the substitute structure used in the method of analysis are included in this report.

2. Description of the Model

A general view of the physical model used to approximate the actual arch is shown in Fig. 1. The model is similar to that presented in Ref. 1*, with the exception that the continuous arch is replaced by ten bars of equal horizontal projections instead of ten bars of equal length. With this arrangement the computation of the instantaneous distribution of the load over the arch is simplified. The bars are considered to be massless and rigid in both bending and axial deformation; the displacements and angle changes are defined at the joints.

The lumped mass at any joint j is given by the equation

$$m_j = \mu \frac{l_j + l_{j+1}}{2}$$

where l_j is the length of the jth bar and μ is the mass per unit length of the continuous arch.

Similarly the stiffness of the flexible joint at j is derived from the elastic properties of the actual arch between mid-points of consecutive panels and is given by the equation

$$K_j = \frac{2\,EI}{l_j + l_{j+1}}$$

where K_j is the stiffness of joint j, E is the elastic modulus, and I is the moment of inertia of the cross section of the arch.

The bars of the analogous framework are numbered consecutively starting with j = 0 at the left hinge and terminating with j = 10 at the right

* "Response of Arches under Dynamic Loads," by R.T. Eppink and A.S. Veletsos, University of Illinois Project, AFSWC - TR-60-53, Air Force Special Weapons Center, Kirtland Air Force Base, New Mexico, December 1960.

hinge, as shown in Fig. 1. Bars are numbered in the same order from 1 to 10, with the bar connecting joints j-1 and j designated as bar j. The total central opening angle of the arch is denoted by φ_o. The deformed configuration of the arch axis is defined with respect to the undeformed shape in terms of the radial and tangential components of the joint displacements. For joint j these are designated as w_j and v_j, respectively. The displacement w_j is considered as positive radially inward, and v_j positive clockwise, as indicated in Fig. 1. The rotations of the bars are considered positive in a clockwise sense.

3. Method of Analysis

The method of analysis is based on the modal analysis technique as applied to the substitute structure. The data required for such an analysis include the natural frequencies and modes of vibration of the model. Since the distribution of the pressure along the arch varies with time, the participation factors for the various modes are time-dependent quantities. The analysis presented here is restricted to the elastic range, and buckling tendencies are ignored. In other words, the results are valid only for small values of p_o/p_{cr}, where p_{cr} is the buckling pressure of the arch.

The computation of the response involves the following steps:

i. Determination of the natural frequencies and modes of the substitute structure.

ii. Determination of the load distribution across the arch at any time.

iii. Computation of the modal participation factors corresponding to a discrete system of time intervals, the time increment chosen being small enough to yield solutions which are reasonably accurate. Such a computation involves the derivation of the governing participation factor equation for

each mode. An approximate marching type of procedure was adopted for the solution of the participation factor equation. In this procedure, the instantaneous participation factors and their time derivatives for each mode are obtained by use of the appropriate quantities at the previous time instant.

iv. Superposition of the modes at any time instant considering the respective participation factors.

In this report the details of the procedures are omitted. All solutions were obtained on the ILLIAC, the digital computer of the University of Illinois.

4. Numerical Solutions

4.1 Problem Parameters. The properties of the arch are specified in terms of the following parameters:

Φ_o = the total opening angle of the arch.

L_o/r = the ratio of the span of the arch to the radius of gyration of the cross-section of the arch, referred to as the slenderness ratio.

The load parameters are defined with respect to the fundamental breathing period, T_o, of a complete ring of the same radius and thickness. This period is given by the equation

$$T_o = 2\pi\sqrt{\frac{mR^2}{AE}}$$

The load parameters are

$$\frac{t_d}{T_o} = \frac{\text{Duration of the blast pulse}}{\text{Breathing period of the complete ring}}$$

$$\frac{t_t}{T_o} = \frac{\text{Time of travel of the peak pressure front over the arch span}}{\text{Breathing period of the complete ring}}$$

4.2 Problems Considered. Numerical solutions were obtained for the following values of the parameters:

$\varphi_o = 60^o$, $L_o/r = 100$, $t_t/T_o = 1$, $t_d/T_o = 2$ and 5

$\varphi_o = 60^o$, $L_o/r = 50$, $t_t/T_o = 1$, $t_d/T_d = 2$ and 5

$\varphi_o = 90^o$, $L_o/r = 100$, $t_t/T_o = 1.5$, $t_d/T_d = 3$ and 7.5

$\varphi_o = 90^o$, $L_o/r = 50$, $t_t/T_o = 1.5$, $t_d/T_o = 3$ and 7.5

In all cases the time interval of integration was taken as $0.05\ T_o$.

The response of the arch was evaluated for the following conditions:

(i) Considering all eighteen modes of vibration

(ii) considering the first antisymmetrical mode and the first and second symmetrical modes. The latter solution will be referred to as the three-mode solution. In addition, for several of the problems, solutions were obtained considering only two modes of vibration. The combinations considered included the first symmetrical and the first antisymmetrical modes, or the second symmetrical and the first antisymmetrical modes. Finally, some solutions were obtained by considering the first two symmetrical and the first two antisymmetrical modes. In this report only a few of these solutions are presented.

4.3 Comparison of Solutions Obtained by Two Different Methods. As a check on the accuracy of the computer program used to obtain the numerical data presented herein, in Figs. 3 and 4 the time histories of the displacements, moments, and thrusts determined by the eighteen mode solution are compared with those determined by application of the method described in the reference listed on p. 2.2. These results are for an arch with $\varphi_o = 60^o$ and $L_o/r = 100$. The first four circular natural frequencies and the corresponding

modes of vibration of this arch are shown in Fig. 2. It can be seen that there is fairly good agreement between the two solutions, the maximum difference for the peak values of displacements, moments, and thrusts being less than 3 percent. The phase difference between the two solutions is due to the slightly different procedures employed in the two methods to concentrate the external pressure at the node points.

4.4 Presentation and Discussion of Results. For each of the problems enumerated above, the solutions were studied to determine the combination of modes which best approximated the eighteen mode solution. Since the arch model considered has eighteen degrees of freedom, the eighteen mode solution represents the exact solution. In general, it was found that the solution based on the first antisymmetrical mode and the first two symmetrical modes provided a very good approximation to the true response.

In Figs. 5 through 14 are given the time histories of the response curves for displacements, moments, and axial forces at selected points of the arch for several of the problems considered. Both the three mode solution and the eighteen mode solution are presented. It can be seen that the two sets of solutions are consistently in good agreement. The best agreement is obtained for displacements and axial forces. The moment curves are influenced to a greater extent by the higher modes than either the deflection or the axial force curves.

For displacements, reasonable agreement was also obtained by considering only the first symmetrical and the first antisymmetrical modes. However, the results for moment and axial forces were generally unsatisfactory. The solutions based on the first antisymmetrical mode and the second sym-

metrical mode were generally no better than the two mode solution referred to above. For displacements and moments, the greatest contribution to the response was provided by the first antisymmetrical mode.

5. Summary

The results of this study indicate that a satisfactory method of analysis for arches under moving pressures can be developed by considering only the first antisymmetrical and the first two symmetrical natural modes of vibration.

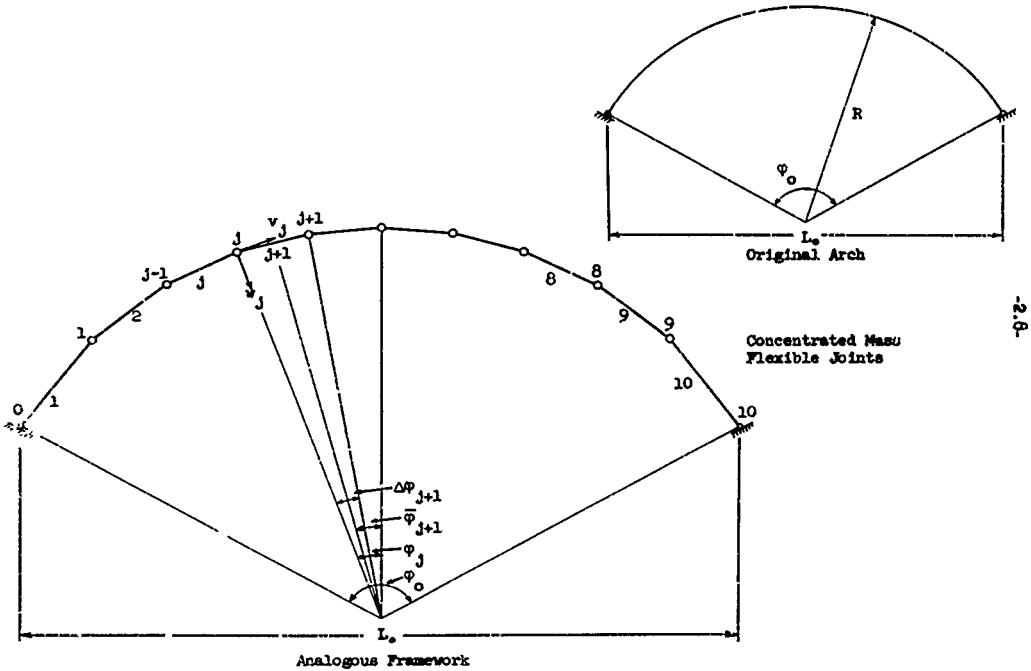

FIG. 1 STRUCTURE CONSIDERED IN THE ANALYSIS

First Anti-symmetrical Mode; $\omega = 32.14\sqrt{\frac{EI}{\mu L_o^4}}$

First Symmetrical Mode; $\omega = 66.63\sqrt{\frac{EI}{\mu L_o^4}}$

Second Anti-symmetrical Mode; $\omega = 124.08\sqrt{\frac{EI}{\mu L_o^4}}$

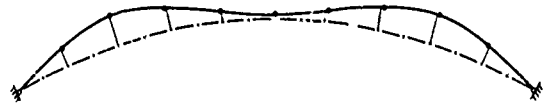

Second Symmetrical Mode; $\omega = 98.48\sqrt{\frac{EI}{\mu L_o^4}}$

FIG. 2 NATURAL MODES OF VIBRATION; $\varphi_o = 60$, $L_o/r = 100$

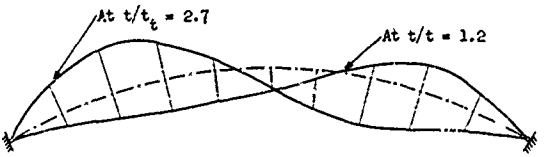

(a) Displacement Configurations

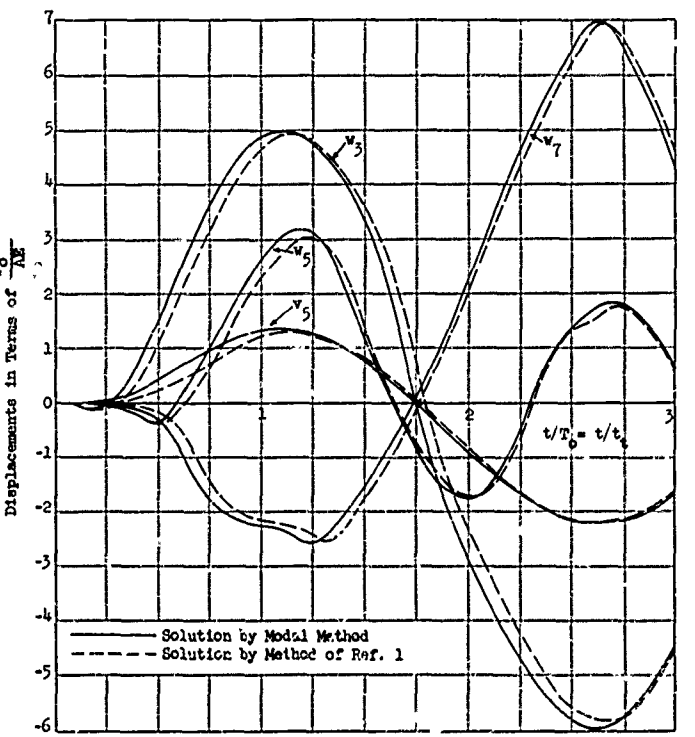

(b) Time Histories of Displacements

FIG. 3 TIME HISTORIES OF RADIAL AND TANGENTIAL DISPLACEMENTS
$\Phi_o = 60^\circ$, $L_o/r = 100$, $t_d/T_o = 2$, $t_r/T_o = 1$, $\Delta t/T_o = .05$

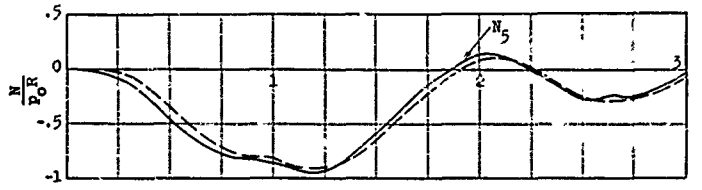

(a) Axial Force, N

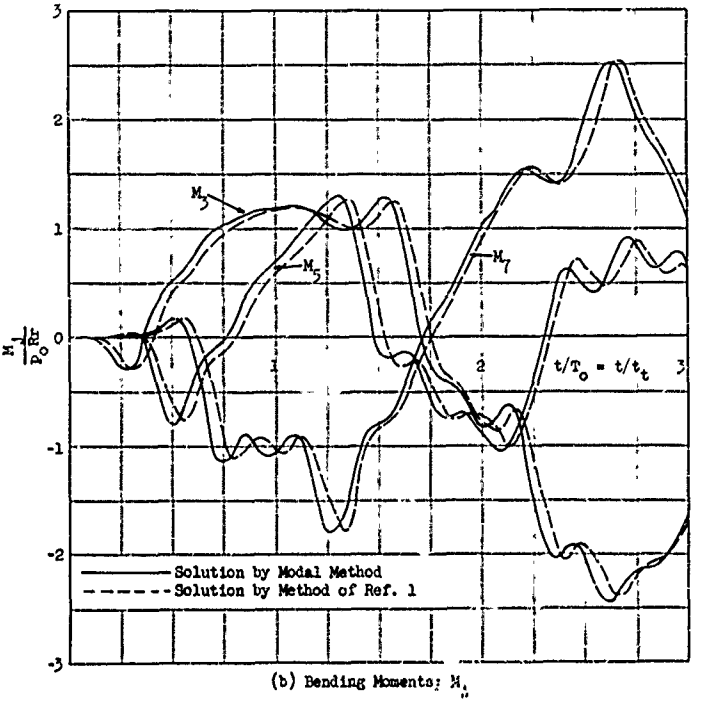

(b) Bending Moments, M_1

FIG. 4 TIME HISTORIES OF AXIAL FORCE AND BENDING MOMENTS
$\varphi_o = 60^\circ$, $L_o/r = 100$, $t_d/T_o = 2$, $t_t/T_o = 1$, $\Delta t/T_o = .05$

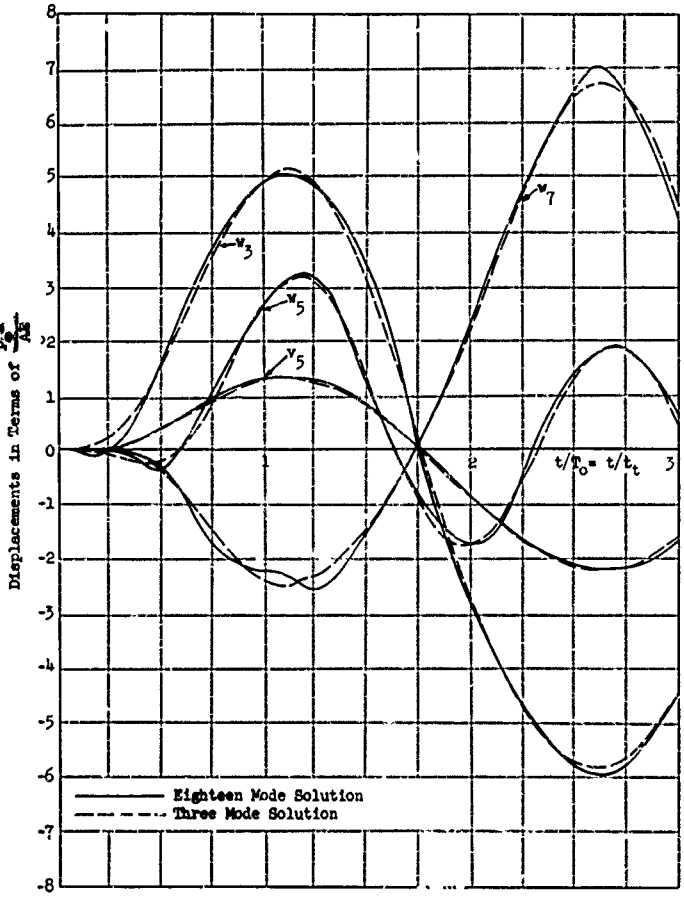

FIG. 5 COMPARISON OF THE DISPLACEMENTS OBTAINED BY EIGHTEEN MODE SOLUTION AND THE THREE MODE SOLUTION

$\varphi_o = 60^\circ$, $L_o/r = 100$, $t_d/T_o = 2$, $t_t/T_o = 1$, $\Delta t/T_o = .05$

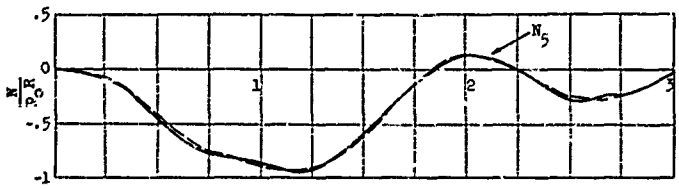

(a) Axial Force; N

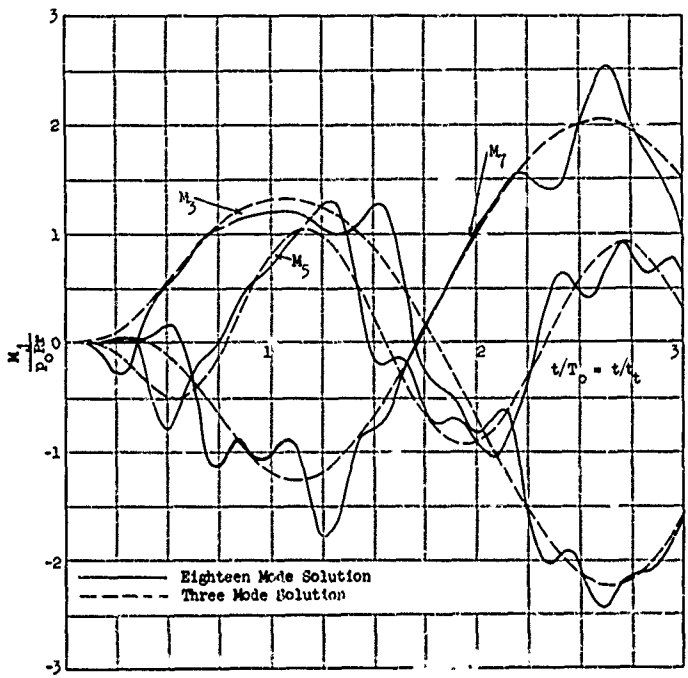

(b) Bending Moments; M_j

FIG. 6 COMPARISON OF AXIAL FORCE AND BENDING MOMENTS
$\varphi = 60^o$, $L_o/r = 100$, $t_d/T_o = 1$, $\frac{\Delta t}{T_o} = .05$

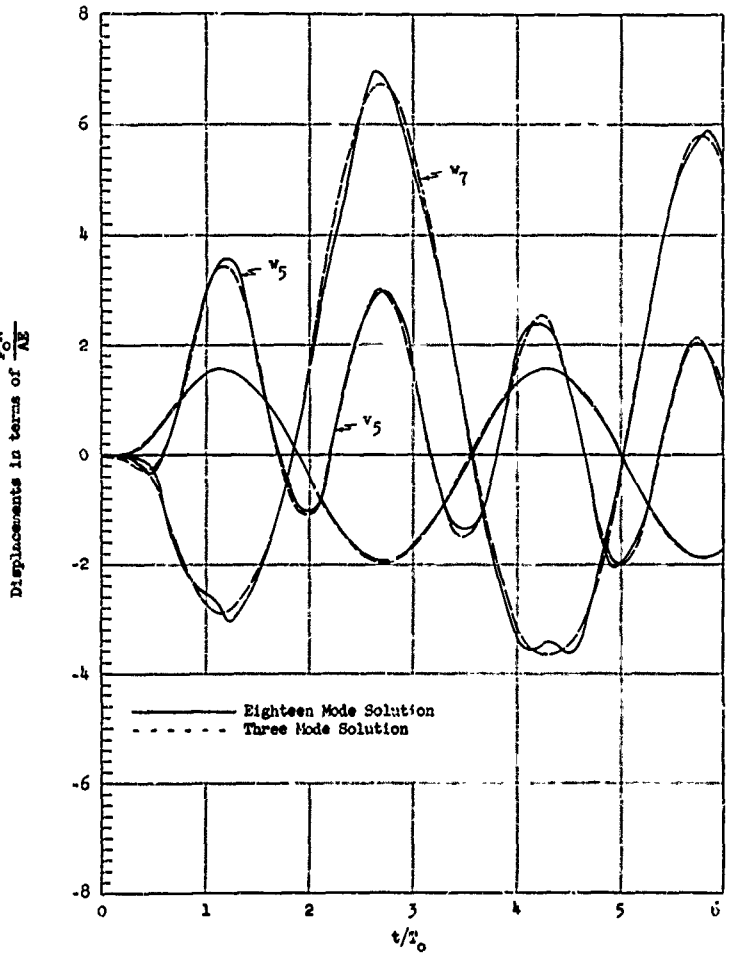

FIG. 7 RESPONSE CURVES FOR DISPLACEMENTS
$\Phi_o = 60^0$, $L_o/r = 100$, $t_t/T_o = 1$,
$t_d/T_o = 5$

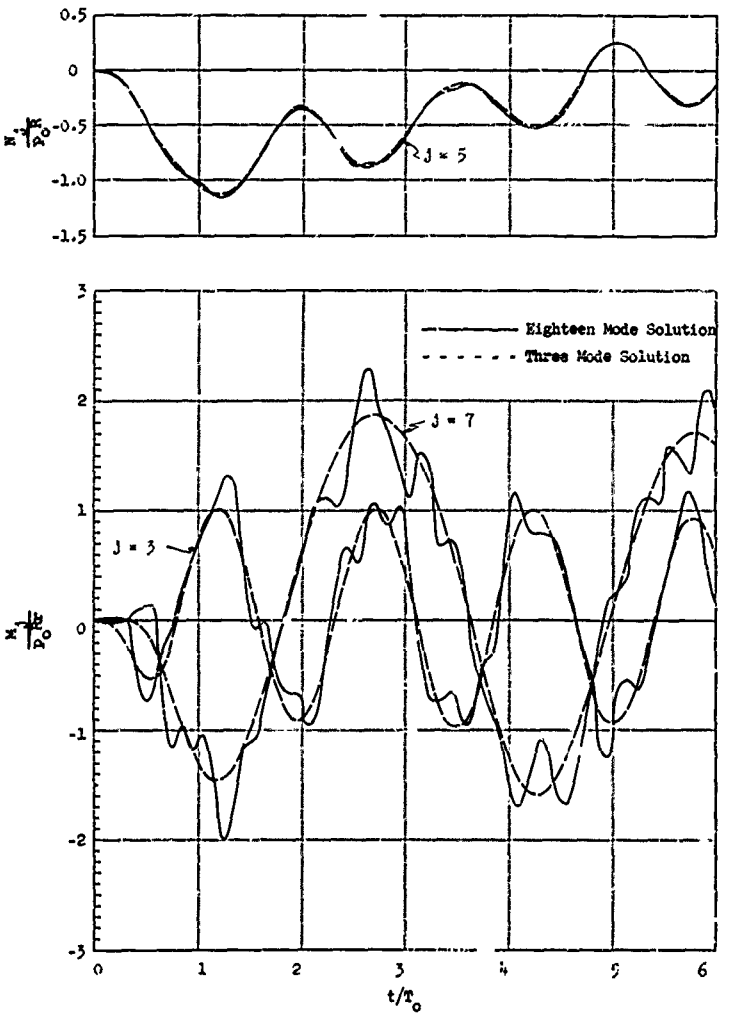

FIG. 8 RESPONSE CURVES FOR AXIAL FORCE AND BENDING MOMENTS
$\varphi_o = 60^\circ$, $L_o/r = 100$, $t_t/t_o = 1$, $t_t/T_o = 5$

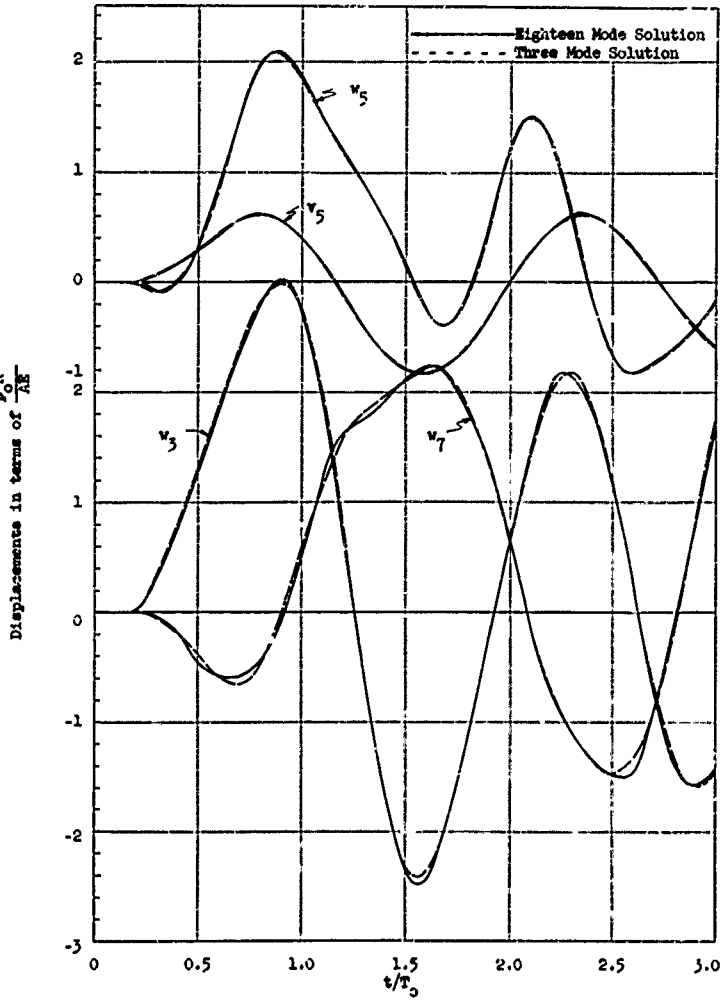

FIG. 9 RESPONSE CURVES FOR DISPLACEMENTS
$\varphi_o = 60^\circ$, $L_o/r = 50$, $t_t/T_o = 1$,
$t_d/T_o = 2$

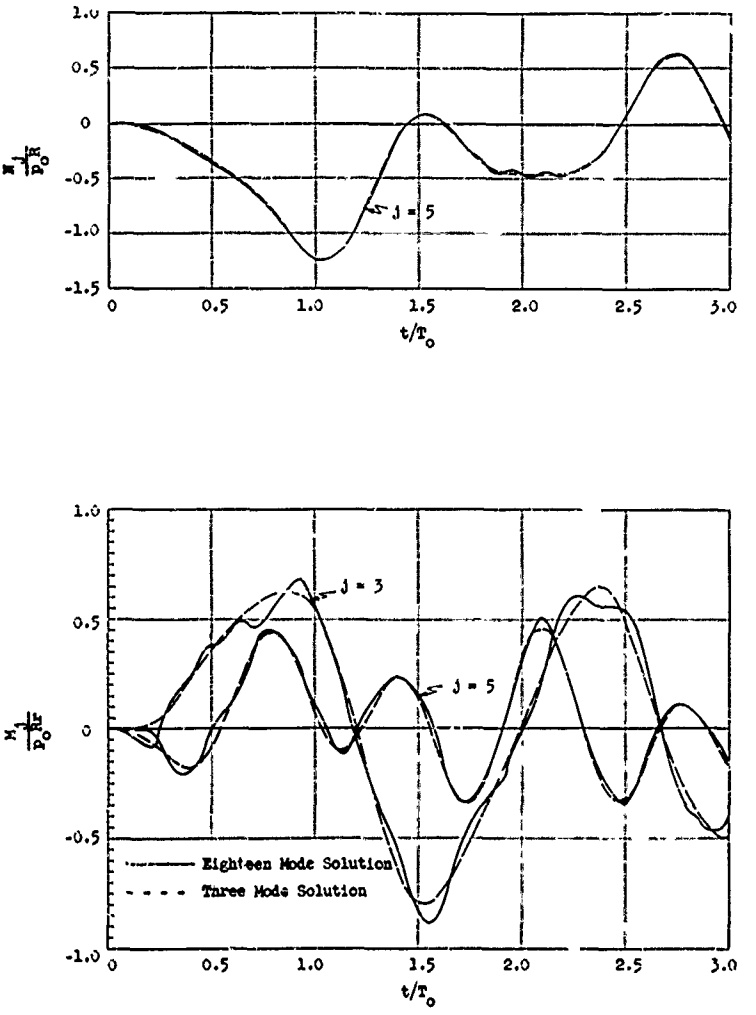

FIG. 10 RESPONSE CURVES FOR AXIAL FORCE AND BENDING MOMENTS
$\varphi_o = 60^o$, $L_o/r = 50$, $t_t/T_o = 1$, $t_d/T_o = 2$

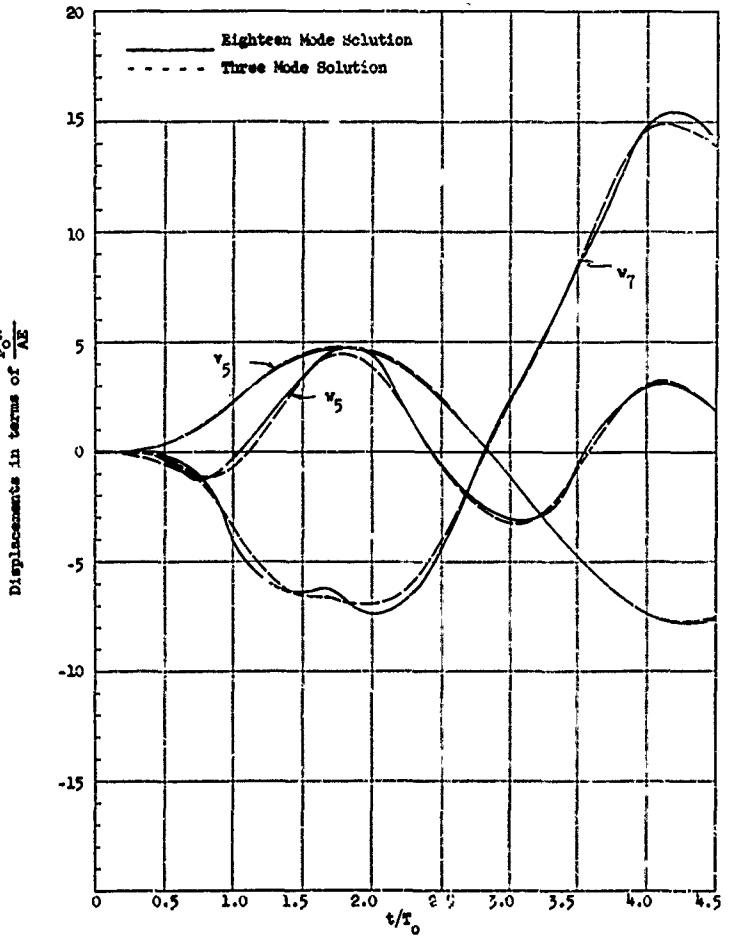

FIG. 11 RESPONSE CURVES FOR DISPLACEMENTS
$\gamma_o = 90^o$, $L_o/r = 100$, $t_t/T_o = 1.5$,
$t_d/T_o = 3$

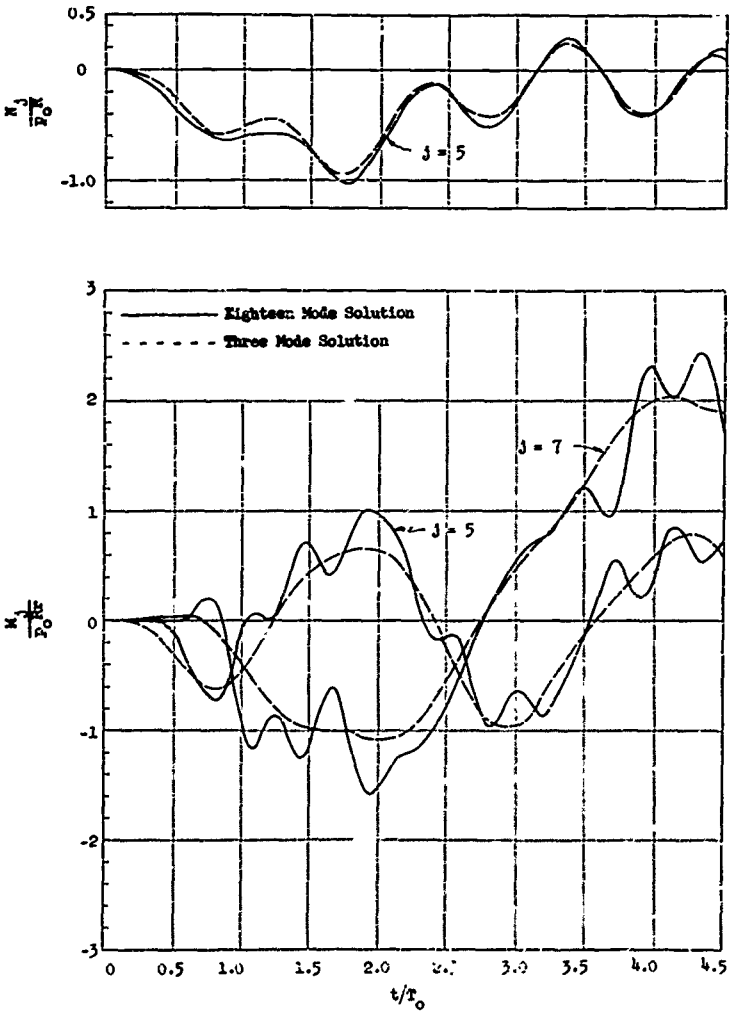

FIG. 12 RESPONSE CURVES FOR AXIAL FORCE AND MOMENTS
$\varphi = 90^\circ$, $L_o/r = 100$, $t_t/T_o = 1.5$,
$t_d/T_o = 3$

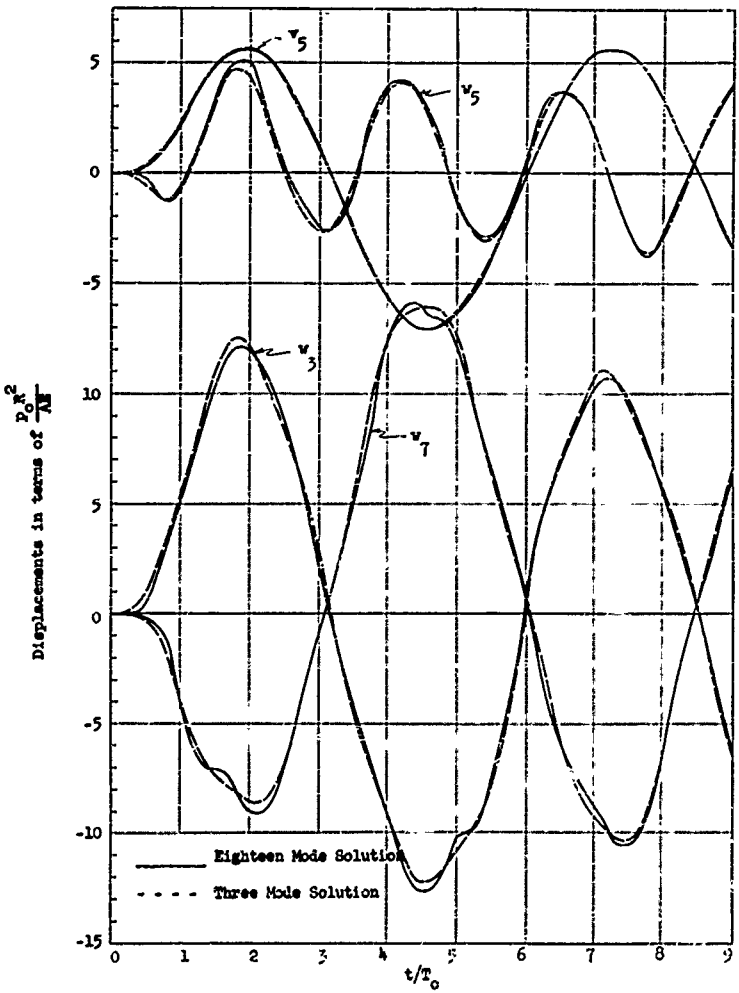

FIG. 13 RESPONSE CURVES FOR DISPLACEMENTS
$\varphi_o = 90^o$, $L_o/r = 100$, $t_t/T_o = 1.5$,
$t_d/T_o = 7.5$

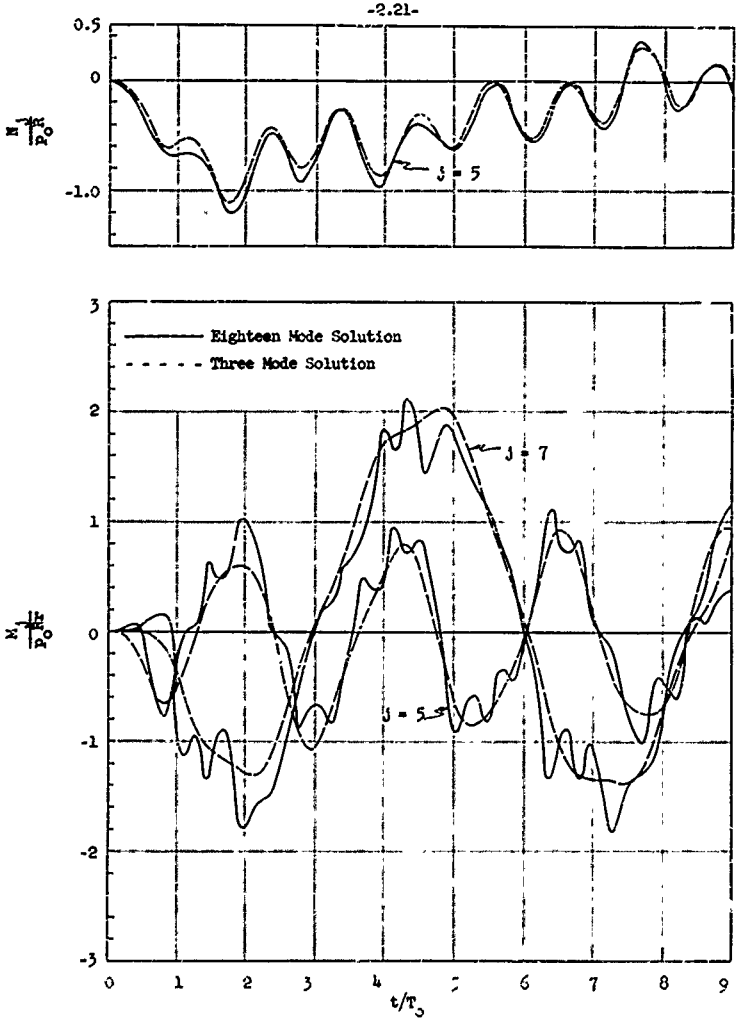

FIG. 14 RESPONSE CURVES FOR AXIAL FORCE AND MOMENTS
$\Phi = 90^{\circ}$, $L_o/r = 100$, $t_t/T_o = 1.5$,
$t_d/T_o = 7.5$

PART III

AN APPROXIMATE THEORY FOR THE LARGE DEFLECTIONS OF UNSYMMETRICALLY LOADED SPHERICAL SHELLS

by

R. L. Jennings

Approved by

A. R. Robinson

AN APPROXIMATE THEORY FOR THE LARGE DYNAMIC DEFLECTIONS OF UNSYMMETRICALLY LOADED THIN SPHERICAL SHELLS

Introduction

Presented herein is a general theory for the large deflections, but small strains, of spherical shells loaded unsymmetrically by time-varying, external pressures. Three equations in three displacement unknowns are developed by a variational procedure employing Hamilton's Principle of Least Action.

The strain energy function used in the formulation of the total energy of the shell is developed under the assumption that the state of stress is approximately plane; that is, the effect of transverse shear stress and of transverse normal stress, acting on surfaces parallel to the middle surface, may be neglected. This assumption yields the usual Hooke's Law relations used in ordinary plate theory.

The law of deformation of a fiber of the shell is governed by the Kirchoff-Love Assumptions which state that (a) points lying on a normal to the undeformed middle surface remain on the same normal to the deformed middle surface, and (b) the displacements in the direction of the normal to the middle surface are approximately equal for all points on the same normal.

These assumptions restrict the following analysis to thin shells ($\frac{h}{a} \leq \frac{1}{20}$). However, the equations of motion include the effects of rotatory inertia.

In the following development, the external pressure is assumed to be caused by air blast, and is always directed normal to the outer surface of the shell.

The significant contributions of this study include the retention of all the important nonlinear terms in the strain-displacement relations,

and a rigorous calculation of the potential energy of the external pressure to make possible the consideration of "dynamic instability."

Exact Strain-Displacement Relations

The complete strain-displacement relations for a spherical dome have been derived earlier,[2] and are summarized here for convenient reference. The position of any point on the shell in its undeformed state is defined by the orthogonal curvilinear coordinates (θ,φ,z). The displacement vector (u,v,w) is chosen such that u and v are tangent to the θ and φ coordinate lines, while w is directed outward along the surface normal (see Fig. 1).

In the following relations, subscripts on u, v, w indicate partial derivatives, while subscripts on ϵ and γ indicate the direction of the strain component. The radial distance to a point of the shell, a + z, is denoted by r.

$$\epsilon_{\theta\theta} = \frac{1}{r}(u_\theta + w) + \frac{1}{2r^2}\left[(u_\theta + w)^2 + (v_\theta - u)^2 + (v_\theta^2)\right]$$

$$\epsilon_{\varphi\varphi} = \frac{1}{r}(u\cot\theta + \frac{v_\varphi}{\sin\theta} + w)$$

$$+ \frac{1}{2r^2}\left[(u\cot\theta + \frac{v_\varphi}{\sin\theta} + w)^2 + (\frac{u_\varphi}{\sin\theta} - v\cot\theta)^2 + (\frac{v_\varphi}{\sin\theta} - v)^2\right]$$

$$\epsilon_{zz} = w_z + \frac{1}{2}\left[(u_z)^2 + (v_z)^2 + (w_z)^2\right]$$

$$\gamma_{\theta\varphi} = \frac{1}{r}(v_\theta + \frac{u_\varphi}{\sin\theta} - v\cot\theta)$$

$$+ \frac{1}{r^2}\left[(u_\theta + w)(\frac{u_\varphi}{\sin\theta} - v\cot\theta) + (v_\theta + \frac{v_\varphi}{\sin\theta} - v)\right.$$

$$\left. + (v_\theta)(\frac{v_\varphi}{\sin\theta} + u\cot\theta + w)\right] \qquad (3)$$

$$\gamma_{\theta z} = (u_z + \frac{w_\theta}{r} - \frac{u}{r}) + \frac{1}{r}\left[(u_z)(u_\theta + w) + (v_z)(v_\theta) + (w_z)(w_\theta - u)\right]$$

$$\gamma_{\varphi z} = (v_z + \frac{w_\varphi}{r \sin\theta} - \frac{v}{r}) \qquad (1)$$

$$+ \frac{1}{r}\left[(u_z)(\frac{u_\varphi}{\sin\theta} - v\cot\theta) + (v_z)(\frac{v_\varphi}{\sin\theta} + u\cot\theta + w) + (w_z)(\frac{w_\varphi}{\sin\theta} - v)\right]$$

Assumption about Displacement Variation Through Thickness

The usual assumption in beams, plates and shells that normals remain normal, straight and inextensional in the deformed state is used here. This assumption about middle surface normals leads to the result that the displacement vector (u,v,w) varies linearly with z through the shell thickness. Thus we have:

$$\begin{aligned} u(\theta,\varphi,z) &= u_0(\theta,\varphi,0) + z\,\psi_0(\theta,\varphi,0) \\ v(\theta,\varphi,z) &= v_0(\theta,\varphi,0) + z\,\delta_0(\theta,\varphi,0) \\ w(\theta,\varphi,z) &= w_0(\theta,\varphi,0) \end{aligned} \qquad (2)$$

where (u_0, v_0, w_0) is the displacement vector of a point on the middle surface at $z = 0$. ψ_0 is the rotation of the normal in the meridional plane. δ_0 is the rotation of this normal in a plane normal to the meridional plane. If the rotations of the normal are small, $w(z)$ will not differ markedly from $w(z=0)$, and so w is assumed to be independent of ψ and δ.

The rotations of the normal are determined from the Kirchoff-Love Assumptions. For the normal to remain straight during deformation, no shear deformation may take place. This requires that

$$\gamma_{\theta z} = \gamma_{\varphi z} = 0 \qquad (3)$$

Substitution of Equations (1) and (2) into Eq. (3) yields two simultaneous equations relating ψ, δ and their derivatives.

$$\psi\,(a+w+u_\theta+z\psi_\theta) + \delta\,(v_\theta+z\delta_\theta) = u - w_\theta$$

$$\psi\left(\frac{u_\varphi}{\sin\theta} + \frac{z\,\psi_\varphi}{\sin\theta} - v\cot\theta - z\,\delta\cot\theta\right) \tag{3a}$$

$$+\,\delta\left(a+\frac{v_\varphi}{\sin\theta} + \frac{z\,\delta_\varphi}{\sin\theta} + u\cot\theta + z\,\psi\cot\theta + w\right) = v - \frac{w_\varphi}{\sin\theta}$$

Since ψ and δ are independent of z, their values are required to satisfy the auxiliary conditions: $\psi\psi_\theta + \delta\delta_\theta = \psi\psi_\varphi + \delta\delta_\varphi = 0$. An approximate solution to Eqs. (3a) is

$$\psi = \frac{u-w_\theta}{a+w+u_\theta}\,, \qquad \delta = \frac{v - \dfrac{w_\varphi}{\sin\theta}}{a+w+u\cot\theta + \dfrac{v_\varphi}{\sin\theta}} \tag{3b}$$

Finally, to facilitate the derivation of the equations of motion, we approximate Eq. (3b) as

$$\psi = \frac{u-w_\theta}{a}\,, \qquad \delta = \frac{v - \dfrac{w_\varphi}{\sin\theta}}{a} \tag{4}$$

Approximate Strain-Displacement Relations

From the three-dimensional expression for Hooke's Law, the requirement that $\sigma_z = 0$ results in

$$\sigma_z = 0 = \frac{E}{(1+\nu)(1-2\nu)}\left[(1-\nu)\,\epsilon_z + (\nu)(\epsilon_\theta + \epsilon_\varphi)\right]$$

which gives

$$\epsilon_z = \frac{-\nu}{1-\nu}\,(\epsilon_\theta+\epsilon_\varphi) \tag{5}$$

Thus it is necessary only to evaluate ϵ_θ, ϵ_φ and $\gamma_{\theta\varphi}$ directly. Substitution of Eqs. (2) and (4) into (1) results in (retaining only nonlinear terms in v and its derivatives):

$$\epsilon_\theta = \left(\frac{u_\theta}{a} - \frac{z}{a+z}\frac{w_{\theta\theta}}{a} + \frac{w}{a+z}\right)$$

$$+ \frac{1}{2(a+z)^2}\left[\left(w - \frac{z}{a}w_{\theta\theta}\right)^2 + (a+z)^2\left(\frac{v_\theta}{a}\right)^2 + \frac{z^2}{a^2\sin^2\theta}\left(w_{\theta\varphi} - v_\varphi\cot\theta\right)^2\right] \tag{6}$$

$$\epsilon_\varphi = \left(\frac{u\cot\theta}{a} + \frac{v_\varphi}{a\sin\theta} + \frac{w}{a+z} - \frac{z}{a+z}\frac{w_\theta\cot\theta}{a} - \frac{z}{a+z}\frac{v_{\varphi\varphi}}{a\sin^2\theta}\right)$$

$$+ \frac{1}{2(a+z)^2}\left[\left(w - \frac{z}{a}w_\theta\cot\theta - \frac{z}{a}\frac{w_{\varphi\varphi}}{\sin^2\theta}\right)^2 + (a+z)^2\left(\frac{v_\varphi}{a\sin\theta}\right)^2\right. \tag{7}$$

$$\left. + \frac{z^2}{a^2\sin^2\theta}\left(v_\varphi\cot\theta - w_{\theta\varphi}\right)^2\right]$$

$$\gamma_{\theta\varphi} = \left(\frac{u_\varphi}{a\sin\theta} + \frac{v_\theta}{a} - \frac{v\cot\theta}{a} - \frac{2z}{a+z}\frac{w_{\theta\varphi}}{a\sin\theta} + \frac{2z}{a+z}\frac{w_\varphi\cot\theta}{a\sin\theta}\right)$$

$$+ \frac{1}{2(a+z)^2}\left[(a+z)^2\left(\frac{w_\theta w_\varphi}{a^2\sin\theta}\right) + z\left(w - \frac{z}{a}w_{\theta\theta}\right)\left(\frac{w_\varphi\cot\theta}{a\sin\theta} - \frac{w_{\theta\varphi}}{a\sin\theta}\right)\right. \tag{8}$$

$$\left. + z\left(\frac{v_\varphi\cot\theta}{a\sin\theta} - \frac{w_{\theta\varphi}}{a\sin\theta}\right)\left(w - \frac{z}{a}\frac{w_{\varphi\varphi}}{\sin^2\theta} - \frac{z}{a}w_\theta\cot\theta\right)\right]$$

The term $1/a+z$ may be expanded as:

$$\frac{1}{a+z} = \frac{1}{a}\left(1 - \frac{z}{a} + \frac{z^2}{a^2} - \ldots\right) \tag{9}$$

$$\left(\frac{1}{a+z}\right)^2 = \frac{1}{a^2}\left(1 - 2\frac{z}{a} + 3\frac{z^2}{a^2} - \ldots\right) \tag{10}$$

and the principal strains may be expressed in the form:

$$\begin{aligned}\epsilon_\theta &= (A + Bz + Cz^2 + \ldots)\\ \epsilon_\varphi &= (D + Fz + Hz^2 + \ldots)\\ \gamma_{\varphi\varphi} &= (J + Kz + Lz^2 + \ldots)\end{aligned} \tag{11}$$

Following the suggestion of Langhaar,[1] the expansions for the strains are cut off after the linear term in z. Substitution of Eqs. (9) and (10) into Eqs. (6), (7) and (8) then yields (retaining only derivatives of w):

$$
\begin{aligned}
A &= \frac{1}{a}(u_\theta + w) + \frac{w_\theta^2}{2a^2} \\
B &= -\frac{1}{a^2}(w + w_{\theta\theta}) \\
D &= \frac{1}{a}\left(u\cot\theta + \frac{v_\varphi}{\sin\theta} + w\right) + \frac{w_\varphi^2}{2a^2\sin^2\theta} \\
F &= -\frac{1}{a^2}\left(w + w_\theta\cot\theta + \frac{w_{\varphi\varphi}}{\sin^2\theta}\right) \\
J &= \frac{1}{a}\left(\frac{u_\varphi}{\sin\theta} + v_\theta - v\cot\theta\right) + \frac{w_\theta w_\varphi}{2a^2\sin^2\theta} \\
K &= \frac{2}{a^2\sin\theta}\left(w_\varphi\cot\theta - w_{\theta\varphi}\right)
\end{aligned}
\tag{12}
$$

Stress Resultants

In the case of plane stress, the elastic stress-strain relations assume the form:

$$
\sigma_\theta = \frac{E}{1-\nu^2}\left[\epsilon_\theta + \nu\,\epsilon_\varphi\right], \quad \sigma_\varphi = \frac{E}{1-\nu^2}\left[\epsilon_\varphi + \nu\,\epsilon_\theta\right], \quad \tau_{\theta\varphi} = \frac{E}{2(1+\nu)}\,\gamma_{\theta\varphi} \tag{13}
$$

Substitution of Eqs. (11) and (13) into the following stress resultant formulas results in:

$$
N_\theta = \int_{-\frac{h}{2}}^{\frac{h}{2}} \sigma_\theta\left(1 + \frac{z}{a}\right) dz = \frac{Eh}{1-\nu^2}\left[(A+\nu D) + \frac{h^2}{12a}(B+\nu F)\right] \tag{14}
$$

$$
N_\varphi = \int_{-\frac{h}{2}}^{\frac{h}{2}} \sigma_\varphi\left(1 + \frac{z}{a}\right) dz = \frac{Eh}{1-\nu^2}\left[(D+\nu A) + \frac{h^2}{12a}(F+\nu B)\right] \tag{15}
$$

$$N_{\theta\varphi} = N_{\varphi\theta} = \int_{-\frac{h}{2}}^{\frac{h}{2}} \tau_{\theta\varphi}\left(1+\frac{z}{a}\right) dz = \frac{Eh}{2(1+\nu)}\left[J + \frac{h^2}{12a}(K)\right] \tag{16}$$

$$M_\theta = \int_{-\frac{h}{2}}^{\frac{h}{2}} z\sigma_\theta\left(1+\frac{z}{a}\right) dz = \frac{Eh^3}{12(1-\nu^2)}\left[(B+\nu F) + \frac{1}{a}(A+\nu D)\right] \tag{17}$$

$$M_\varphi = \int_{-\frac{h}{2}}^{\frac{h}{2}} z\sigma_\varphi\left(1+\frac{z}{a}\right) dz = \frac{Eh^3}{12(1-\nu^2)}\left[(F+\nu B) + \frac{1}{a}(D+\nu A)\right] \tag{18}$$

$$M_{\theta\varphi} = M_{\varphi\theta} = \int_{-\frac{h}{2}}^{\frac{h}{2}} z\tau_{\theta\varphi}\left(1+\frac{z}{a}\right) dz = \frac{Eh^3}{24(1+\nu)}\left[K + \frac{1}{a}(J)\right] \tag{19}$$

Strain Energy

For small strains, the elastic strain energy of deformation is given by the volume integral:

$$U = \frac{1}{2}\int_{-\frac{h}{2}}^{\frac{h}{2}} \int_0^{2\pi} \int_0^{\bar{\theta}} \left[\sigma_\theta\epsilon_\theta + \sigma_\varphi\epsilon_\varphi + \tau_{\theta\varphi}\gamma_{\theta\varphi}\right](a+z)^2 \sin\theta \, d\theta d\varphi dz \tag{20}$$

this can be expressed in terms of strains only by use of Eqs (13).

$$U = \frac{E}{2(1-\nu^2)}\int_{-\frac{h}{2}}^{\frac{h}{2}} \int_0^{2\pi} \int_0^{\bar{\theta}} \left[(\epsilon_\theta^2+\epsilon_\varphi^2) + 2\nu\,\epsilon_\theta\epsilon_\varphi + \left(\frac{1-\nu}{2}\right)\gamma_{\theta\varphi}^2\right] (a+z)^2 \sin\theta \, d\theta d\varphi dz \tag{21}$$

Replacing the strains by Eqs. (11) and performing the integration, we have:

$$U = U_1 + U_2 + U_3 \tag{22}$$

where:

$$U_1 = \frac{Eha^2}{2(1-\nu^2)}\int_0^{2\pi}\int_0^{\bar{\theta}}\left[A^2+D^2+2\nu AD + \left(\frac{1-\nu}{2}\right)J^2\right]\sin\theta \, d\theta d\varphi \tag{23}$$

$$U_2 = \frac{Eh^3a^2}{24(1-\nu^2)}\int_0^{2\pi}\int_0^{\bar{\theta}}\left[B^2+F^2+2\nu BF + \left(\frac{1-\nu}{2}\right)K^2\right]\sin\theta \, d\theta d\varphi \tag{24}$$

$$U_3 = \frac{Eh^3}{24(1-\nu^2)} \int_0^{2\pi} \int_0^{\bar{\theta}} \left\{ \begin{array}{l} \left[A^2+D^2+2\nu AD + \left(\frac{1-\nu}{2}\right) J^2\right] \\ + 4\varepsilon\left[AB+DF+\nu(AF+BD)+\left(\frac{1-\nu}{2}\right)JK\right] \end{array} \right\} \sin\theta \, d\theta d\Phi \tag{25}$$

U_1 is the membrane strain energy due to stretching of the middle surface. U_2 is the usual expression for the flexural strain energy used in most theories of thin shells. U_3 is a correction to the bending energy due to the inclusion of the term $(a+z)^2$ instead of a^2 in Eq. (21).

Kinetic Energy

The kinetic energy is given by the volume integral

$$T = \frac{\rho}{2} \int_{-\frac{h}{2}}^{\frac{h}{2}} \int_0^{2\pi} \int_0^{\bar{\theta}} \left[(u_t + z\psi_t)^2 + (v_t + z\delta_t)^2 + (w_t)^2\right](a+z)^2 \sin\theta \, d\theta d\Phi dz \tag{26}$$

Potential Energy of External Pressure

During deformation, the elastic strain energy changes. Also, the external pressure does work, and the corresponding change of energy must be included in the expression for the total energy.

The external pressure is considered to be caused by air blast. As such it is directed normal to the outer surface of the shell. The potential energy of the external pressure is then given as:

$$\Omega = -\iiint q \, \Delta(dV) \tag{27}$$

where $\Delta(dV)$ is the change of an infinitesimal element of volume. Since the geometry of the shell is specified in polar coordinates (θ,Φ), it is convenient to use these coordinates in specifying the volume change. An infinitesimal element of shell volume is expressed as:

$$dV = \rho^2 \sin\theta_D \, d\theta_D \, d\Phi_D \, d\rho$$

where ρ is the distance from the center of undeformed curvature to a point on the outer surface. Calling $\bar{\rho}_D$ the distance to a point on the deformed outer surface, and $\bar{\rho}_u$ the distance to a point on the undeformed outer surface, the potential energy of the external pressure becomes:

$$\Omega = -\frac{1}{3}\int_0^{2\pi}\int_0^{\bar{\theta}} q\left[\bar{\rho}_D^3 \sin\theta_D \, d\theta_D \, d\varphi_D - \bar{\rho}_u^3 \sin\theta \, d\theta d\varphi\right] \tag{28}$$

where:

$$\begin{aligned} \bar{\rho}_D &= \sqrt{(a + \tfrac{h}{2} + w^*)^2 + (u^*)^2 + (v^*)^2} \\ \bar{\rho}_u &= a + \tfrac{h}{2} \end{aligned} \tag{29}$$

and the angles locating the deformed point are approximately:

$$\theta_D \cong \theta + \left[\left(\frac{u^*}{a + \frac{h}{2} + w^*}\right) - \frac{1}{3}\left(\frac{u^*}{a + \frac{h}{2} + w^*}\right)^3 + \ldots\right] \tag{30}$$

$$\varphi_D \cong \varphi + \left[\left(\frac{v^*}{[a + \frac{h}{2} + w^*]\sin\theta + u^*\cos\theta}\right) - \frac{1}{3}\left(\frac{v^*}{[a + \frac{h}{2} + w^*]\sin\theta + u^*\cos\theta}\right)^3 + \ldots\right]$$

where the starred quantities indicate displacements on the outer surface, $z = \frac{h}{2}$. Equations (30) indicate that θ_D and φ_D do not depend on the squares of the displacements. Thus, we retain only the linear terms in these expressions, and have:

$$\begin{aligned} d\theta_D &= d\theta + \frac{\partial}{\partial\theta}\left[\frac{u^*}{a + \frac{h}{2} + w^*}\right] d\theta \\ d\varphi_D &= d\varphi + \frac{\partial}{\partial\varphi}\left[\frac{v^*}{(a + \frac{h}{2} + w^*)\sin\theta + u^*\cos\theta}\right] d\varphi \end{aligned} \tag{31}$$

These relations are approximate, and based on the assumption that θ_D is a function of θ only, and φ_D is a function of φ only. With the relation that

$$\sin\theta_D = \sin\left[\theta + \frac{u^*}{a + \frac{h}{2} + w^*}\right] = \sin\theta\left[\cos\left(\frac{u^*}{a + \frac{h}{2} + w^*}\right)\right. \\ \left. + \cot\theta \sin\left(\frac{u^*}{a + \frac{h}{2} + w^*}\right)\right] \tag{32}$$

the potential energy express on becomes:

$$\Omega = -\frac{1}{3}\int_0^{2\pi}\int_0^{\bar{\theta}} q\left\{\left[\left(a + \frac{h}{2} + w^*\right)^2 + u^{*2} + v^{*2}\right]^{\frac{3}{2}}\left[\cos x + \cot\theta \sin x\right]\right. \\ \left.\left[1 + \frac{\partial x}{\partial\theta}\right]\left[1 + \frac{\partial y}{\partial\varphi}\right] - \left[a + \frac{h}{2}\right]^3\right\}\sin\theta \, d\theta d\varphi \tag{33}$$

where: $x = \dfrac{u^*}{a + \frac{h}{2} + w^*} \simeq \dfrac{u^*}{a + \frac{h}{2}}$

$$y = \frac{v^*}{(a + \frac{h}{2} + w^*)\sin\theta + u^* \cos\theta} \simeq \frac{v^*}{(a + \frac{h}{2})\sin\theta}$$

Finally the integrand may be expanded by using the following approximations:

$$\left[\left(a + \frac{h}{2} + w^*\right)^2 + (u^*)^2 + (v^*)^2\right]^{\frac{3}{2}} \simeq \left(a + \frac{h}{2} + w^*\right)^3 + \frac{3}{2}\left(a + \frac{h}{2} + w^*\right)\left[(u^*)^2 + (v^*)^2\right]$$

$$\cos x = \cos\left(\frac{u^*}{a + \frac{h}{2} + w^*}\right) \simeq 1 - \frac{1}{2}\left(\frac{u^*}{a + \frac{h}{2} + w^*}\right)^2 \simeq 1 - \frac{1}{2}\left(\frac{u^*}{a + \frac{h}{2}}\right)^2$$

$$\sin x = \sin\left(\frac{u^*}{a + \frac{h}{2} + w^*}\right) \simeq \frac{u^*}{a + \frac{h}{2} + w^*} \simeq \frac{u^*}{a + \frac{h}{2}}$$

$$\left(1 + \frac{\partial x}{\partial\theta}\right)\left(1 + \frac{\partial y}{\partial\varphi}\right) \simeq \left(1 + \frac{u_\theta^*}{a + \frac{h}{2}}\right)\left(1 + \frac{v_\varphi^*}{[a + \frac{h}{2}]\sin\theta}\right) \simeq 1 + \frac{u_\theta^* + v_\varphi^*/\sin\theta}{a + \frac{h}{2}} \\ + \frac{u_\theta^* \, v_\varphi^*}{(a + \frac{h}{2})^2 \sin\theta}$$

Substitution of these approximate relations into Eq. (33) results in the following expression for the potential energy ($\Omega^* = w$):

$$\Omega = -\frac{1}{3}\int_0^{2\pi}\int_0^{\bar{\theta}} q\left\{(a+\frac{h}{2}+w)(k_1)(k_2)(k_3) - (a+\frac{h}{2})^3\right\}\sin\vartheta\, d\theta d\varphi \qquad (34)$$

where: $$k_1 = (a+\frac{h}{2}+w)^2 + \frac{1}{2}(u^*)^2 + \frac{1}{2}(v^*)^2 \qquad (35)$$

$$k_2 = 1 + \frac{u^*\cot\theta}{a+\frac{h}{2}} - \frac{1}{2}\left(\frac{u^*}{a+\frac{h}{2}}\right)^2 \qquad (36)$$

$$k_3 = 1 + \frac{u_\theta{}^x + \frac{v_\varphi{}^*}{\sin\theta}}{a+\frac{h}{2}} + \frac{u_\vartheta{}^x\, v_\varphi{}^*}{(a+\frac{h}{2})^2\sin\theta} \qquad (37)$$

Equations of Motion

The principle of virtual work, when extended to a dynamics problem yields the useful relation

$$\int_{t_0}^{t_1}(\delta T - \delta U - \delta\Omega)\, dt = 0 \qquad (38)$$

This is often referred to as "Hamilton's Principle." For a conservative system, Eq. (38) becomes

$$\delta\int_{t_0}^{t_1}(T - U - \Omega)\, dt = 0 \qquad (39)$$

Equation (39) implies that among all motions that will carry a conservative system from a given configuration x_0 to a given configuration x_1 in a given time interval (t_0,t_1), that which actually occurs provides a stationary value to the integral. The significance of Eq. (39) is that the Euler-Lagrange equations for the integral are the differential equations of motion for the system under consideration.

Substitution of energy functions from Eqs. (23), (24), (25), (26), and (34) into Eq. (39) yields the following variational equation:

$$\delta\int_{t_0}^{t_1}\int_0^{2\pi}\int_0^{\bar{\theta}}\left\{\begin{array}{l}\frac{\rho}{2}\int_{-\frac{h}{2}}^{\frac{h}{2}}(a+z)^2\left[(u_t+z\psi_t)^2+(v_t+z\delta_t)^2+(w_t)^2\right]dz\\ -\frac{Eha^2}{2(1-\nu^2)}\left[A^2+D^2+2\nu AD+\left(\frac{1-\nu}{2}\right)J^2\right]\\ -\frac{Eh^3a^2}{24(1-\nu^2)}\left[B^2+F^2+2\nu BF+\left(\frac{1-\nu}{2}\right)K^2\right]\\ -\frac{Eh^3}{24(1-\nu^2)}\left[\left\{A^2+D^2+2\nu AD+\left(\frac{1-\nu}{2}\right)J^2\right\}\right.\\ \left.+4a\left\{AB+DF+\nu(AF+BD)+\left(\frac{1-\nu}{2}\right)JK\right\}\right]\\ +\frac{q}{3}\left[(a+\frac{h}{2}+w)(k_1k_2k_3)-(a+\frac{h}{2})^3\right]\end{array}\right\}\sin\theta\ d\theta d\varphi dt = 0 \qquad (40)$$

which becomes

$$\delta\int_{t_0}^{t_1}\int_0^{2\pi}\int_0^{\bar{\theta}}\left\{\begin{array}{l}\frac{\rho a^2h}{2}\left[\begin{array}{l}(1+\epsilon_a)(u_t^2+v_t^2)+(1+n)(w_t^2)+n\left(v_{\theta t}^2+\frac{v_{\varphi t}^2}{\sin^2\theta}\right)\\ -6n\left(u_tw_{\theta t}+\frac{v_tw_{\varphi t}}{\sin\theta}\right)\end{array}\right]\sin\theta\\ -\frac{Eha^2}{2(1-\nu^2)}\left[A^2+D^2+2\nu AD+\left(\frac{1-\nu}{2}\right)J^2\right]\sin\theta\\ -\frac{Eh^3a^2}{24(1-\nu^2)}\left[B^2+F^2+2\nu BF+\left(\frac{1-\nu}{2}\right)K^2\right]\sin\theta\\ -\frac{Eh^3}{24(1-\nu^2)}\left[\left\{A^2+D^2+2\nu AD+\left(\frac{1-\nu}{2}\right)J^2\right\}\right.\\ \left.+4a\left\{AB+DF+\nu(AF+BD)+\left(\frac{1-\nu}{2}\right)JK\right\}\right]\sin\theta\\ +\frac{q}{3}\left[(a+\frac{h}{2}+w)(k_1k_2k_3)-(a+\frac{h}{2})^3\right]\sin\theta\end{array}\right\}d\theta d\varphi dt=0 \qquad (41)$$

where $n = \frac{h^2}{12a^2}$.

Designating the integrand of Eq. (41) by the symbol "f," the Euler-Lagrange Equations assume the form:

$$\frac{\partial f}{\partial u} - \frac{\partial}{\partial \theta}\left(\frac{\partial f}{\partial u_\theta}\right) - \frac{\partial}{\partial \varphi}\left(\frac{\partial f}{\partial u_\varphi}\right) - \frac{\partial}{\partial t}\left(\frac{\partial f}{\partial u_t}\right) = 0 \tag{42}$$

$$\frac{\partial f}{\partial v} - \frac{\partial}{\partial \theta}\left(\frac{\partial f}{\partial v_\theta}\right) - \frac{\partial}{\partial \varphi}\left(\frac{\partial f}{\partial v_\varphi}\right) - \frac{\partial}{\partial t}\left(\frac{\partial f}{\partial v_t}\right) = 0 \tag{43}$$

$$\begin{aligned}\frac{\partial f}{\partial w} - \frac{\partial}{\partial \theta}\left(\frac{\partial f}{\partial w_\theta}\right) - \frac{\partial}{\partial \varphi}\left(\frac{\partial f}{\partial w_\varphi}\right) - \frac{\partial}{\partial t}\left(\frac{\partial f}{\partial w_t}\right) + \frac{\partial^2}{\partial \theta^2}\left(\frac{\partial f}{\partial w_{\theta\theta}}\right) + \frac{\partial^2}{\partial \varphi^2}\left(\frac{\partial f}{\partial w_{\varphi\varphi}}\right) \\ + \frac{\partial^2}{\partial t^2}\left(\frac{\partial f}{\partial w_{tt}}\right) + \frac{\partial^2}{\partial \theta \partial \varphi}\left(\frac{\partial f}{\partial w_{\theta\varphi}}\right) + \frac{\partial^2}{\partial \theta \partial t}\left(\frac{\partial f}{\partial w_{\theta t}}\right) + \frac{\partial^2}{\partial \varphi \partial t}\left(\frac{\partial f}{\partial w_{\varphi t}}\right) = 0\end{aligned} \tag{44}$$

Performing the operations indicated in Eqs. (42), (43), and (44) results in three nonlinear partial differential equations in three unknowns (u,v,w). Many of the terms in these equations may be replaced by their symbolic representation as stress resultants. These three equations, in terms of stress resultants are presented below.

$$\begin{aligned}&\frac{\partial}{\partial \theta}\left(aN_\theta + M_\theta\right) + \frac{1}{\sin\theta}\frac{\partial}{\partial \varphi}\left(aN_{\theta\varphi} + M_{\theta\varphi}\right) + \cot\theta\left[a(N_\theta - N_\varphi) + (M_\theta - M_\varphi)\right] \\ &= \rho h^3\left[u_{tt}\left(\frac{a^2}{h^2} + \frac{1}{5}\right) - \frac{w_{\theta tt}}{4}\right] - \frac{1}{\sin\theta}\left[\frac{\partial Q}{\partial u} - \frac{\partial}{\partial \theta}\left(\frac{\partial Q}{\partial u_\theta}\right) - \frac{\partial}{\partial \varphi}\left(\frac{\partial Q}{\partial u_\varphi}\right)\right]\end{aligned} \tag{45}$$

$$\begin{aligned}&\frac{\partial}{\partial \theta}\left(aN_{\theta\varphi} + M_{\theta\varphi}\right) + \frac{1}{\sin\theta}\frac{\partial}{\partial \varphi}\left(aN_\varphi + M_\varphi\right) + 2\cot\theta\left[aN_{\theta\varphi} + M_{\theta\varphi}\right] \\ &= \rho h^3\left[v_{tt}\left(\frac{a^2}{h^2} + \frac{1}{2}\right) - \frac{w_{\varphi tt}}{4\sin\theta}\right] - \frac{1}{\sin\theta}\left[\frac{\partial Q}{\partial v} - \frac{\partial}{\partial \theta}\left(\frac{\partial Q}{\partial v_\theta}\right) - \frac{\partial}{\partial \varphi}\left(\frac{\partial Q}{\partial v_\varphi}\right)\right]\end{aligned} \tag{46}$$

$$\frac{\partial^2}{\partial\theta^2}\left[\sin\theta\,(M_\theta + anN_\theta)\right] + \frac{\partial^2}{\partial\varphi^2}\left[\frac{1}{\sin\theta}\,(M_\varphi + anN_\varphi)\right]$$

$$+ 2\,\frac{\partial^2}{\partial\theta\partial\varphi}\left[M_{\theta\varphi} + anN_{\theta\varphi}\right] - \sin\theta\left[n\,(M_\theta + M_\varphi) + a\,(N_\theta + N_\varphi)\right]$$

$$+ \frac{\partial}{\partial\theta}\left[\frac{w_\theta \sin\theta}{a}\,(M_\theta + aN_\theta) + \frac{w_\varphi}{2\,a\sin\theta}\,(M_{\theta\varphi} + aN_{\theta\varphi}) - \cos\theta\,(M_\varphi + anN_\varphi)\right]$$

$$+ \frac{\partial}{\partial\varphi}\left[\frac{w_\varphi}{a\sin\theta}\,(M_\varphi + aN_\varphi) + \frac{w_\theta}{2\,a\sin\theta}\,(M_{\theta\varphi} + aN_{\theta\varphi}) + 2\cot\theta(M_{\theta\varphi} + anN_{\theta\varphi})\right]$$

$$= \rho h^3 \sin\theta\left[w_{tt}\left(\frac{a^2}{h^2} + \frac{1}{12}\right) + \frac{1}{4}\,(u_{tt}\cot\theta + u_{\theta tt} + \frac{v_{\varphi tt}}{\sin\theta})\right.$$

$$\left. - \frac{1}{12}\,(w_{\theta tt}\cot\theta + w_{\theta\theta tt} + \frac{w_{\varphi\varphi tt}}{\sin^2\theta})\right]$$

$$- \left[\frac{\partial Q}{\partial w} - \frac{\partial}{\partial\theta}\left(\frac{\partial Q}{\partial w_\theta}\right) - \frac{\partial}{\partial\varphi}\left(\frac{\partial Q}{\partial w_\varphi}\right) + \frac{\partial^2}{\partial\theta^2}\left(\frac{\partial Q}{\partial w_{\theta\theta}}\right) + \frac{\partial^2}{\partial\varphi^2}\left(\frac{\partial Q}{\partial w_{\varphi\varphi}}\right) + \frac{\partial^2}{\partial\theta\partial\varphi}\left(\frac{\partial Q}{\partial w_{\theta\varphi}}\right)\right] \tag{47}$$

where: $$Q = \frac{q\sin\theta}{\beta}\,(a + \frac{h}{2} + w)(k_1k_2k_3) \tag{48}$$

In the limit, where $n \longrightarrow 0$, and where the nonlinearity of Eq. (47) is neglected, these equations assume the form:

$$\frac{\partial}{\partial\theta}\,(aN_\theta + M_\theta) + \frac{1}{\sin\theta}\,\frac{\partial}{\partial\varphi}\,(aN_{\theta\varphi} + M_{\theta\varphi}) + \cot\theta\left[a(N_\theta - N_\varphi) + (M_\theta - M_\varphi)\right]$$

$$= \rho\, ha^2\, u_{tt} \tag{49}$$

$$\frac{\partial}{\partial\theta}\,(aN_{\theta\varphi} + M_{\theta\varphi}) + \frac{1}{\sin\theta}\,\frac{\partial}{\partial\varphi}\,(aN_\varphi + M_\varphi) + 2\cot\theta\left[aN_{\theta\varphi} + M_{\theta\varphi}\right] = \rho ha^2\, v_{tt} \tag{50}$$

$$\frac{\partial^2 M_\theta}{\partial\theta^2} + \frac{1}{\sin^2\theta}\,\frac{\partial^2 M_\varphi}{\partial\varphi^2} + \frac{2}{\sin\theta}\,\frac{\partial^2 M_{\theta\varphi}}{\partial\theta\partial\varphi} + 2\cot\theta\,\frac{\partial M_\theta}{\partial\theta} - \cot\theta\,\frac{\partial M_\varphi}{\partial\theta}$$

$$+ \frac{2\cot\theta}{\sin\theta}\,\frac{\partial M_{\theta\varphi}}{\partial\varphi} + \left[(M_\varphi - M_\theta) - a(N_\theta + N_\varphi)\right] = \rho ha^2\, w_{tt} \tag{51}$$

The left-hand sides of Eqs. (49), (50), and (51) are in the same form as those derived by Flügge[3] by static equilibrium considerations.

Equations (45) through (47), when coupled with the stress resultant formulas yield three equations in three unknowns. These equations include nonlinear, large-displacement effects, rotatory inertia effects, and the effects of change of geometry on the dynamic equilibrium of the system.

This change of geometry effect enters in two ways. It enters all three equations through the energy of the external pressure on a shell surface whose area changes with time. It also enters the equation for radial equilibrium, Eq. (47), due to the large deformation effect which alters the line of action of the stress resultants. This latter effect is observed only in Eq. (47) because only nonlinear terms in w and its derivatives have been retained in Eqs. (12).

The nonlinear equations are too lengthy to express here in displacement form, however, the linearized Eqs. (49) through (51) are presented here:

$$(1+n)\Big[u_{\theta\theta} + u_\theta \cot\theta + \left(\tfrac{1-\nu}{2}\right)\frac{u_{\varphi\varphi}}{\sin^2\theta} - u(\nu + \cot^2\theta) + \left(\tfrac{1+\nu}{2}\right)\frac{v_{\theta\varphi}}{\sin\theta} - \left(\tfrac{3-\nu}{2}\right)\frac{v_\varphi \cot\theta}{\sin\theta} + w_\theta(1+\nu)\Big] - n\left[w_{\theta\theta\theta} + w_{\theta\theta}\cot\theta + w_\theta(1-\cot^2\theta) + \frac{v_{\theta\varphi\varphi}}{\sin^2\theta} - \frac{2w_{\varphi\varphi}\cot\theta}{\sin^2\theta}\right] - \frac{u_{tt}}{\omega_0^2} = 0 \qquad (52)$$

$$(1+n)\Big[\left(\tfrac{1+\nu}{2}\right)\frac{u_{\theta\varphi}}{\sin\theta} + \left(\tfrac{3-\nu}{2}\right)u_\varphi\frac{\cos\theta}{\sin^2\theta} + \frac{v_{\varphi\varphi}}{\sin^2\theta} + \left(\tfrac{1-\nu}{2}\right)(v_{\theta\theta} + v_\theta\cot\theta + v - v\cot^2\theta) + (1+\nu)\frac{w_\varphi}{\sin\theta}\Big] - n\Big[\frac{v_{\theta\theta\varphi}}{\sin\theta} + \frac{v_{\varphi\varphi\varphi}}{\sin^3\theta} + w_{\theta\varphi}\frac{\cot\theta}{\sin\theta} + \frac{2w_\varphi}{\sin\theta}\Big] - \frac{v_{tt}}{\omega_0^2} = 0 \qquad (53)$$

$$(1+n)(1+\nu)\left[u\cot\theta + u_\theta + \frac{v_\varphi}{\sin\theta} + 2w\right]$$

$$- n\Big[u_{\theta\theta\theta} + 2u_{\theta\theta}\cot\theta - u_\theta\cot^2\theta + u\cot\theta\,(3+\cot^2\theta) + \frac{u_{\varphi\varphi}\cot\theta}{\sin^2\theta}$$

$$+ \frac{u_{\theta\varphi\varphi}}{\sin^2\theta} + \frac{v_{\theta\theta\varphi}}{\sin\theta} + \frac{v_{\varphi\varphi\varphi}}{\sin^3\theta} - \frac{v_{\theta\varphi}\cot\theta}{\sin\theta} + \frac{v_\varphi}{\sin\theta}(3+\cot^2\theta)$$

$$- w_{\theta\theta\theta\theta} - 2w_{\theta\theta\theta}\cot\theta + w_{\theta\theta}(1+\nu+\cot^2\theta)$$

$$- w_\theta\cot\theta\,(2-\nu+\cot^2\theta) - \frac{w_{\varphi\varphi\varphi\varphi}}{\sin^4\theta} - \frac{w_{\varphi\varphi}}{\sin^2\theta}(3-\nu+4\cot^2\theta)$$

$$- 2\frac{v_{\theta\theta\varphi\varphi}}{\sin^2\theta} + 2v_{\theta\varphi\varphi}\frac{\cot\theta}{\sin^2\theta} + 2w(1+\nu)\Big] + \frac{w_{tt}}{\omega_0^2} = 0 \qquad (54)$$

where: $n = \dfrac{h^2}{12a^2}$ and $\omega_0^2 = \dfrac{E}{\rho a^2(1-\nu^2)}$

Equations (52) through (54) agree exactly with Eqs. 85(a-c) of Ref. (3) except for the omission of a term in Eq. 85(a) of Flügge's text. These equations are adequate to use in the computation of the natural frequencies of the spherical shell. To find the buckling pressures, however, the nonlinear terms of Eqs. (45) through (47) must be added to these equations. Also, the rotatory inertia terms can no longer be omitted.

REFERENCES

(1) H. L. Langhaar, "A Strain-Energy Expression for Thin Elastic Shells," Journal of Applied Mechanics, p. 183, June, 1949.

(2) J. E. Duberg, R. L. Jennings, et al., "Analysis and Design of Domes, Arches, and Shells," Vol. II of Interim Report on Contract No. AF 29(601)-2591, Project No. 1080, Dept. of Civil Engineering, University of Illinois, p. C-6, November, 1960.

(3) W. Flügge, Stresses in Shells, Springer-Verlag, p. 380, 1960.

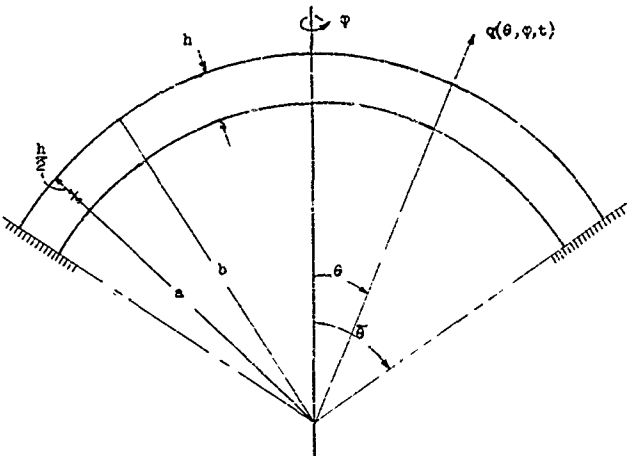

FIG. 1-a SHELL GEOMETRY

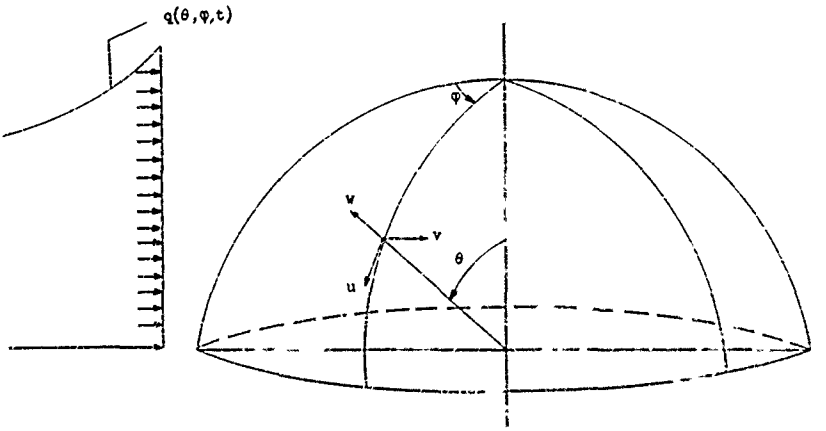

FIG. 1-b NOTATION

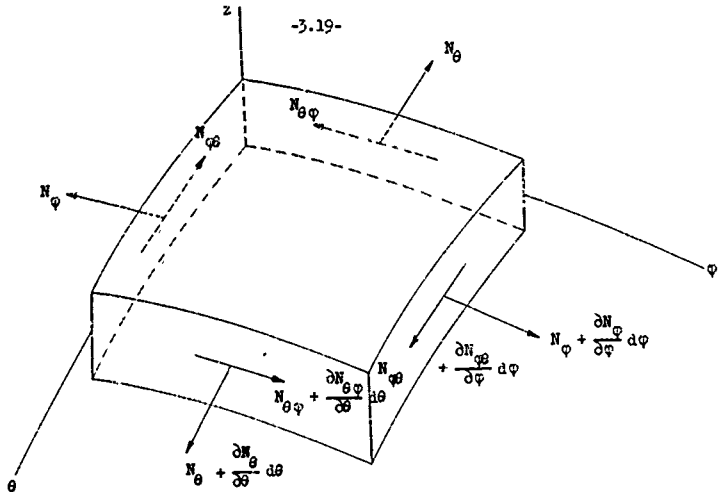

FIG. 2-a MEMBRANE STRESS RESULTANTS

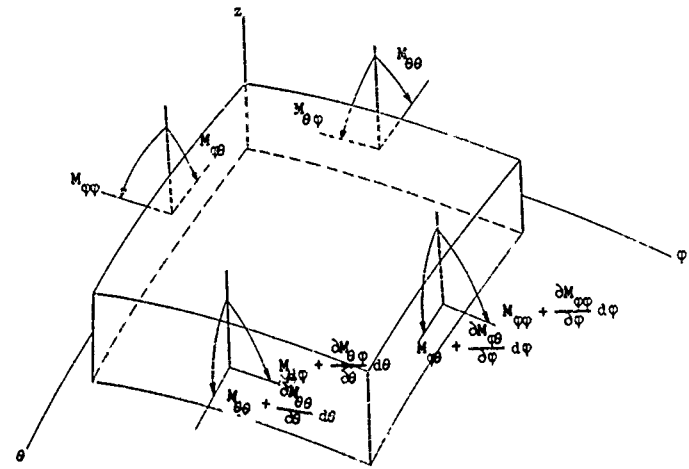

FIG. 2-b FLEXURAL STRESS RESULTANTS

DISTRIBUTION

No. Cys	
	HEADQUARTERS USAF
1	Hq USAF (AFDDC), Wash 25, DC
1	Hq USAF (AFOOA), Wash 25, DC
1	Hq USAF (AFOIE), Wash 25, DC
1	Hq USAF (AFRDR), Wash 25, DC
1	Hq USAF (AFCIN), Wash 25, DC
1	USAF Dep IG for Insp (AFCDI-3-3), Norton AFB, Calif
1	Hq USAF (AFOSR, Tech Library), Bldg T-D, Wash 25, DC
	MAJOR AIR COMMANDS
1	AFSC (SCR), Andrews AFB, Wash 25, DC
1	SAC (DINC), Offutt AFB, Nebr
1	TAC (TDA), Langley AFB, Va
1	AFLC (MCW7), Wright-Patterson AFB, Ohio
1	ADC (Ops Anlys), Ent AFB, Colorado Springs, Colo
1	AUL, Maxwell AFB, Ala
1	USAFA, United States Air Force Academy, Colo
	AFSC ORGANIZATIONS
1	BSD (BSR-VP-3), AF Unit Post Office, Los Angeles 45, Calif
	ASD, Wright-Patterson AFB, Ohio
2	(ASAPRL)
1	(ASMCC)
	KIRTLAND AFB ORGANIZATIONS
	AFSWC, Kirtland AFB, N Mex
1	(SWEH)
26	(SWOI)
3	(SWRS)
	OTHER AIR FORCE AGENCIES
1	Director USAF Project RAND, ATTN: RAND Nuclear Energy Division, via Air Force Liaison Office, The RAND Corporation, 1700 Main Street, Santa Monica, Calif
	ARMY ACTIVITIES
1	Chief of Research and Development, Department of the Army, ATTN: Special Weapons and Air Defense Division, Wash 25, DC

DISTRIBUTION (con't)

No. Cys	
1	Director, Ballistic Research Laboratories, ATTN: Library, Aberdeen Proving Ground, Md
1	Commanding Officer, US Army Engineers, Research and Development Laboratories, Ft. Belvoir, Va
1	Office of the Chief, Corps of Engineers, US Army, ATTN: Protective Construction Branch, Wash 25, DC

NAVY ACTIVITIES

1	Chief, Bureau of Yards and Docks, Department of the Navy, Wash 25, DC
1	Commanding Officer and Director, Naval Civil Engineering Laboratory, Port Hueneme, Calif

OTHER DOD ACTIVITIES

1	Chief, Defense Atomic Support Agency, ATTN: Document Library Branch, Wash 25, DC
1	Commander, Field Command, Defense Atomic Support Agency, ATTN: FCAG3, Sandia Base, N Mex
10	ASTIA (TIPDR), Arlington Hall Sta, Arlington 12, Va
1	Director, Advanced Research Projects Agency, Department of Defense, The Pentagon, Wash 25, DC

OTHER

1	Official Record Copy (SWRS)

AIR FORCE SPECIAL WEAPONS CENTER,
Kirtland Air Force Base, New Mexico
Rpt. No. AFSWC-61-90. STUDIES OF RESPONSES OF ARCHES AND DOMES UNDER DYNAMIC LOADS (U). October 1961.

UNCLASSIFIED Report

This report, consisting of Parts I, II and III, is concerned with three different aspects of the response of arches and domes under dynamic loads. In Part I the accuracy of an approximate design method for arches subjected to dynamic loads is evaluated by comparing the predictions of this method with the exact solutions. Primary emphasis is placed on the effects of loads which are uniformly distributed around the arch. In Part II the response of circular elastic arches under a moving pressure pulse is investigated by the modal method of analysis. Various combinations of natural modes are considered, and the combination of the smallest number of modes

UNCLASSIFIED

1. Blast damage
2. Blast loading
3. Blast model studies
4. Pressure
5. Pressure -- time studies
6. Stress and strain
7. Structural elements - effects of blast

I. AFSC Project 1080, Task 108002
II. Contract AF29(601)-2591
III. Illinois, University, Urbana, Dept. of Civil Engineering
IV. Tseng Huang, S. Iyengar, R.L.Jennings
V. In ASTIA collection

UNCLASSIFIED

AIR FORCE SPECIAL WEAPONS CENTER,
Kirtland Air Force Base, New Mexico
Rpt. No. AFSWC-61-90. STUDIES OF RESPONSES OF ARCHES AND DOMES UNDER DYNAMIC LOADS (U). October 1961.

UNCLASSIFIED Report

This report, consisting of Parts I, II and III, is concerned with three different aspects of the response of arches and domes under dynamic loads. In Part I the accuracy of an approximate design method for arches subjected to dynamic loads is evaluated by comparing the predictions of this method with the exact solutions. Primary emphasis is placed on the effects of loads which are uniformly distributed around the arch. In Part II the response of circular elastic arches under a moving pressure pulse is investigated by the modal method of analysis. Various combinations of natural modes are considered, and the combination of the smallest number of modes

UNCLASSIFIED

1. Blast damage
2. Blast loading
3. Blast model studies
4. Pressure
5. Pressure -- time studies
6. Stress and strain
7. Structural elements - effects of blast

I. AFSC Project 1080, Task 108002
II. Contract AF29(601)-2591
III. Illinois, University, Urbana, Dept. of Civil Engineering
IV. Tseng Huang, S. Iyengar, R.L.Jennings
V. In ASTIA collection

UNCLASSIFIED

AIR FORCE SPECIAL WEAPONS CENTER,
Kirtland Air Force Base, New Mexico
Rpt. No. AFSWC-61-90. STUDIES OF RESPONSES OF ARCHES AND DOMES UNDER DYNAMIC LOADS (U). October 1961.

UNCLASSIFIED Report

This report, consisting of Parts I, II and III, is concerned with three different aspects of the response of arches and domes under dynamic loads. In Part I the accuracy of an approximate design method for arches subjected to dynamic loads is evaluated by comparing the predictions of this method with the exact solutions. Primary emphasis is placed on the effects of loads which are uniformly distributed around the arch. In Part II the response of circular elastic arches under a moving pressure pulse is investigated by the modal method of analysis. Various combinations of natural modes are considered, and the combination of the smallest number of modes

UNCLASSIFIED

1. Blast damage
2. Blast loading
3. Blast model studies
4. Pressure
5. Pressure -- time studies
6. Stress and strain
7. Structural elements - effects of blast

I. AFSC Project 1080, Task 108002
II. Contract AF29(601)-2591
III. Illinois, University, Urbana, Dept. of Civil Engineering
IV. Tseng Huang, S. Iyengar, R.L.Jennings
V. In ASTIA collection

UNCLASSIFIED

AIR FORCE SPECIAL WEAPONS CENTER,
Kirtland Air Force Base, New Mexico
Rpt. No. AFSWC-61-90. STUDIES OF RESPONSES OF ARCHES AND DOMES UNDER DYNAMIC LOADS (U). October 1961.

UNCLASSIFIED Report

This report, consisting of Parts I, II and III, is concerned with three different aspects of the response of arches and domes under dynamic loads. In Part I the accuracy of an approximate design method for arches subjected to dynamic loads is evaluated by comparing the predictions of this method with the exact solutions. Primary emphasis is placed on the effects of loads which are uniformly distributed around the arch. In Part II the response of circular elastic arches under a moving pressure pulse is investigated by the modal method of analysis. Various combinations of natural modes are considered, and the combination of the smallest number of modes

UNCLASSIFIED

1. Blast damage
2. Blast loading
3. Blast model studies
4. Pressure
5. Pressure -- time studies
6. Stress and strain
7. Structural elements - effects of blast

I. AFSC Project 1080, Task 108002
II. Contract AF29(601)-2591
III. Illinois, University, Urbana, Dept. of Civil Engineering
IV. Tseng Huang, S. Iyengar, R.L.Jennings
V. In ASTIA collection

UNCLASSIFIED

which satisfactorily approximates the exact solution is determined. It is concluded that good approximation to the true response can be obtained by considering the contributions of the first antisymmetrical and the first two symmetrical natural modes of vibration. Part III presents a derivation of an approximate theory for the dynamic response of spherical shells loaded unsymmetrically by time-varying pressures. Non-linear effects are considered so that the resulting equations reflect the buckling tendencies associated with large-deflection behavior. UNCLASSIFIED Abstract	UNCLASSIFIED	which satisfactorily approximates the exact solution is determined. It is concluded that good approximation to the true response can be obtained by considering the contributions of the first antisymmetrical and the first two symmetrical natural modes of vibration. Part III presents a derivation of an approximate theory for the dynamic response of spherical shells loaded unsymmetrically by time-varying pressures. Non-linear effects are considered so that the resulting equations reflect the buckling tendencies associated with large-deflection behavior. UNCLASSIFIED Aostract	UNCLASSIFIED
UNCLASSIFIED	UNCLASSIFIED	UNCLASSIFIED	UNCLASSIFIED
which satisfactorily approximates the exact solution is determined. It is concluded that good approximation to the true response can be obtained by considering the contributions of the first antisymmetrical and the first two symmetrical natural modes of vibration. Part II presents a derivation of an approximate theory for the dynamic response of spherical shells loaded unsymmetrically by time-varying pressures. Non-linear effects are considered so that the resulting equations reflect the buckling tendencies associated with large-deflection behavior. UNCLASSIFIED Abstract	UNCLASSIFIED	which satisfactorily approximates the exact solution is determined. It is concluded that good approximation to the true response can be obtained by considering the contributions of the first antisymmetrical and the first two symmetrical natural modes of vibration. Part III presents a derivation of an approximate theory for the dynamic response of spherical shells loaded unsymmetrically by time-varying pressures. Non-linear effects are considered so that the resulting equations reflect the buckling tendencies associated with large-deflection behavior. UNCLASSIFIED Abstract	UNCLASSIFIED